Optimizing the creep response of Additive-manufactured polyethylene terephthalate glycol (PETG) using the Taguchi design of experiment method

Benjamin Auri

Degree Thesis
Mechanical and Sustainability Engineering
2024

Degree Thesis

Benjamin Auri

Optimizing the creep response of Additive-manufactured polyethylene terephthalate glycol (PETG) using the Taguchi design of experiment method

Arcada University of Applied Sciences: Mechanical and Sustainability Engineering, 2024.

Commissioned by:

Arcada University of Applied Sciences

Identification number:

047701935

Abstract

This thesis investigates the influence of 3D printing parameters on the creep response of Polyethylene Terephthalate Glycol (PETG). The tensile test specimens were designed according to ISO 527-1 and manufactured by Fused Filament Fabrication (FFF). Printing parameters that are analysed are, infill geometry: cubic, gyroid, tri hexagonal. Infill orientation: 90, -45/45, 0 °. Infill density: 80, 50, 20 % with nozzle temperatures: 250, 235, 220 $°C$. The Taguchi method was used for the experimental design and testing. After testing, the Signal-to-Noise ratio (SNR) was calculated for each factor. Moreover, the sum of squares (SS) is calculated for each level and factor and an Analysis of Variance (ANOVA) is conducted for determining if the factors and levels are statistically significant. In addition, the creep modulus is calculated and plotted. The results reveal a clear trend of infill density having the largest impact on the creep response of the material, followed by infill geometry and nozzle temperature. The strongest samples, 8 and 6, having 80% infill density with creep modulus values between 1150 MPa-1300 MPa. The weakest samples, 5 and 3, having infill densities of 20% with creep modulus between 690 MPa - 710 MPa. The ANOVA analysis provided a % contribution that each factor had on the creep response. Factor A (infill geometry) had a contribution of 9.7%, factor C (infill density) with a contribution of 85.6% and factor D (nozzle temperature) with a contribution of 4.4%. Factor B (infill orientation) was used as an error term for calculating the f-value and p-values — factor B was considered to have a negligible effect on the creep response. Lastly, the SNR provided the printing parameters which yield the optimal creep behaviour. The printing parameters that yield the best creep response are infill density of 80%, infill geometry cubic, infill orientation of -45/45° and with a nozzle temperature of 235 $°C$.

Keywords:

Taguchi Method, Design of Experiment, ANOVA, Signal-to-Noise, PETG, Infill Density, Infill Orientation, Infill Geometry, Nozzle Temperature, 3D Printing, Creep

Table of Contents

Abbreviation

PETG	Polyethylene Terephthalate Glycol
PET	Polyethylene Terephthalate
DoE	Design of Experiment
PLA	Polylactic Acid
RPLA	Recycled Polylactic Acid
MOT	Modulus of Toughness
ANOVA	Analysis of Variance
CNC	Computer Numerical Control
1.4-CMDH	Cyclo-Hexane-Di-Methanol
NOAA	National Oceanic and Atmospheric Administration
HDPE	High-Density Polyethylene
SNR	Signal-to-Noise Ratio
FSW	Friction Stir Welding
AM	Additive Manufacturing
SM	Subtractive Manufacturing
FFF	Fused Filament Fabrication
MOC	Modulus of Creep

List of symbols

σ	Stress [MPa]
$\dot{\epsilon}$	Strain rate $[\frac{1}{s}]$
$d\varepsilon$	Change in strain [mm]
dt	Change in time [s]

1. Introduction

The world is becoming increasingly mechanized, from tractors replacing drought animals in agriculture [1] to humans using artificial intelligence (AI) as" tools for human labour" [2]. During the last forty years, additive manufacturing has been established for rapid prototype development [3] and for solving complex production, design, and manufacturing issues [4]. In recent years, there has been much focus on the possible applications of 3D printed Polyethylene Terephthalate Glycol (PETG). For instance, prototyping automotive components in particular, interior trims, brackets, and custom accessories for cars [5] as well as applications in modern medicine for tissue engineering, dentistry, drug carriers, and optometry [6].

There has been relatively much research done on the mechanical properties of PETG. Michel Mansour studied the mechanical and dynamic behaviour of 3D-printed PETG reinforced with 20% carbon fibre [7] but left out the creep behaviour of the material. Research carried out by Valvez studied the creep behaviour of 3D printed PETG composites under compression, and found that in comparison with virgin PETG, the yield compressive strength decreased for both Kevlar and carbon-reinforced composites [8]. However, there is a lack of research that has been carried out studying the mechanical properties of creep strain on fused filament fabricated virgin PETG material under a tensile load.

1.1 Aims and Objective

This thesis aims to fill in the gap of research and provide an understanding of what 3D printing parameters provide the optimal creep behaviour for virgin PETG under a tensile load.

There are only a few polymers that are used commonly in additive manufacturing [9]. PETG is a new polymer in the 3D printing industry and displays properties like those of polyethylene terephthalate (PET). Around 70% of all manufactured plastic bottles are made from PET [10], however, PET filament used in 3D printing is highly

brittle, rigid and requires high processing temperatures [11]. The added glycol unit in PETG offers higher flexibility, lowers thermal resistance, and increases adhesion and durability than that of PET which hints that it is a more suitable material for 3D printing.

Creep is a fundamental behaviour in material science which holds especially true for polymers. The desired outcome of this research is to identify which 3D printing parameters have the largest effect on the creep behaviour of PETG. The approach of optimization implemented in this study is similar to research carried out by Pereira [12] , Vespalec [13] and Portoacă [14] by applying Taguchi's design of experiment method (DoE) for optimizing 3D printing processing parameters for enhancing surface quality, wear-resistance, and applied metaobject optimization. The experimental analysis will be done by 3D printing tensile test specimens, following standard ISO 527-2 [1A]:2012.

There are four primary printing parameters analysed each with three levels: infill density (80%, 50% and 20%), infill orientation (90°, -45/45° and 0°), infill geometry (tri hexagonal, gyroid and cubic) with nozzle temperature (220 $°C$, 235$°C$, and 250 $°C$). Furthermore, static tensile creep testing will be carried out using the 350-20 tensile testing machine from Testometric. Optimal creep behaviour will be determined by a single output response method. Similar research conducted by Z. Gebrehiwot on optimising the mechanical properties of recycled polylactic acid (RPLA) by using single and multi-response analyses methods [15]. Gebrehiwot's research concluded that infill orientation was the primary parameter in determining the optimal modulus of toughness (MOT) and tensile strength of the material.

The desired result for creep is as little deformation as possible. Hence, the expected results for good creep behaviour are as followed. Print orientation that is applied in the load direction (90°). Infill density 80% due to infill density largely effecting the tensile load that the material can withstand, the higher the density the more stress that can be applied before deformation. In addition, using tri hexagonal infill geometry has been proven in other studies e.g. S. Ganeshkumar research on 3D-

printed PLA Polymers [16] to be one of the strongest geometries that provide high-yield strength.

The experimental data will be analysed first by calculating the smaller-the-better signal-to-noise ratio (SNR) for each factor and level, to solve for the optimal printing parameters. After, performing an Analysis of Variance (ANOVA) for identifying the key factors and their impact.

Due to PETG being a relatively new polymer, the real-world applications of this research can be very valuable for following researchers, industries and institutions that want to replicate or optimize the experiments. Early research is essential for reducing future costs and identifying possible demerits of the material.

1.2 Objectives of Thesis

1. Successfully apply Taguchi's design of experiment method.

2. Understand the relationship between 3D processing parameters and changes in creep properties of the material.

3. Determine the leading cause for poor and good creep from the mechanical tests and previous research.

4. Apply Analysis of Variance (ANOVA) to reject or confirm the null hypothesis for each factor.

1.3 Compliance with the degree program

This research is an investigation of a polymer and its mechanical properties. When studying at Arcada in the degree program mechanical and sustainability engineer you learn to design and model using 3D modelling software, how to code, and conduct a wide range of computational simulations e.g., FEA, material flow analysis,

stress analysis, etc. As well as structural analysis, dynamic, and statics tests. The research in this thesis, consist of mechanical testing, designing and conducting a well-structured experiment, and 3D printing, all stages relate to the theoretical and hands-on experience that I have gathered during my time at Arcada.

1.4 Ethical issues

All the information about previous research, pictures and methods used in this thesis have been cited and referenced correctly in text and in the reference list. The names of all the researchers, their research as well as companies that are mentioned in this study are all on open platforms. The people who wish to remain anonyms, and their privacy protected have that right and their research and/or names have not been used in order to protect their privacy.

2. Literature review

2.1 Innovation of 3D-printing

The first 3D printer dates to 1981. Dr. Kodama a pioneer in the car and manufacturing industry [17] designed the first rapid prototype machine, this machine could produce parts layer by layer by using resin which UV-light could polymerize [18]. Polymerized resin also known as Polyaddition resin, is synthesized by breaking down the unsaturated bonds that hold It together through an initiator and later combining it again to form a larger stronger polymer bond [19].

3D printing has grown exponentially in the last few decades, and the drive for innovation has shown nothing less, than the capabilities that 3D printing has to offer. 3D printing provides the ability for mass customization, and production of any open-source design within the fields of e.g., agriculture, healthcare, automotive industry, aerospace industries, etc [20]. 3D printing is a form of additive manufacturing which include VAT Polymerization [21], binder jetting [22], and direct energy deposition [23]. Additive manufacturing (AM) is a process of adding layer by layer to form a product. In contrast, laser cutting, water jet cutting, and computer numerical control (CNC) machining are types of manufacturing methods based on material subtraction methods, these kinds of methods are known as subtractive manufacturing (SM) [24]. Subtractive manufacturing tends to need large spaces, requires high amounts of power to operate, and is moderately expensive due to energy utilization, tooling, and machinery [25]. Due to the demerits of subtractive manufacturing, additive manufacturing, specifically 3D printing, has been commercialized and nowadays is a form of manufacturing that can be found in many homes across the globe [26]. Commercialization is related to the innovation of technology, many people want the ability to design 3D models and create products by their bedside, and this, in due course, leads to large amounts of funding and research [27]. The commercialization of 3D printing explains its rapid growth in innovation and technology, and why it is important to search for new materials and methods of optimization.

2.2 Synthesis of PETG

Polyethylene Terephthalate (PET) is a polymer that can be amorphous or semi-crystalline depending on its thermal history [28]. PET is a thermoplastic, invented by two British scientists, John Whinfield and James Dickson, in 1941 [29]. Whinfield and Dickson combined phthalic acid and ethylene glycol to synthesize a material that can be picked and pulled, to form long strong fibres, similar to how Nylon 6,6 is produced [30]. PET is widely used in fabrication due to its high strength and toughness good chemical resistance and can be stretched into a film with strong tensile properties. PET is arguably one of the most important polymers that we have [31]. However, when PET is heated, it crystalizes and turns opaque in colour, which weakens the bonds, for this reason, it is not good for high-temperature applications, such as 3D printing. PET is often copolymerized, modifying the molecular structure of PET by replacing the original ethylene-glycol unit, with, for example 1.4-CycloHexaneDiMethanol (1.4 CHDM) for the synthesis of PETG (polyethylene terephthalate glycol-modified) [32]. The CHDM-unit added to the polymer backbone prevents crystallization at higher temperatures and keeps most of the mechanical properties of PET unaltered, hence, making PETG suitable and a high-quality thermoplastic polymer for applications such as 3D printing [33].

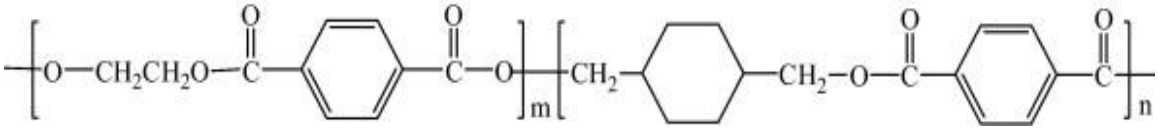

Figure 1 Polyethylene terephthalate copolymerized with 1.4-CycloHexaneDiMethanol (PETG), p. 10 [34]

2.3 Recycling of PETG

Environmental concerns arise when discussing the production of plastics for everyday usage, however these concerns don't discourage the appeal and desire for manufacturing and research of new and more environmentally friendly polymers. Like all plastics, PETG can take decades to degrade in nature, and if left out in the environment, can reduce natural processes, cause harm to wildlife, and prohibit the ecosystem's ability to adapt naturally to climate change, thus directly affecting

millions of lives as stated by the UN environment program on plastic pollution [35]. Microplastics, found in nature, arise from the degradation of larger plastic debris left out in the environment. A study by the National Oceanic and Atmospheric Administration (NOAA) mentioned that plastics are the most common type of marine debris found in our oceans and lakes [36]. PETG filament, if discarded into the environment can be harmful however, PETG is relatively easy to recycle.

Plastics can be categorized into two groups based on their ability to be remelted and reused: thermoplastics and thermosets. Thermosets are highly cross-linked polymers that are infusible and insoluble and considered difficult to recycle [37] they include materials e.g., polyesters, silicone, melamine, Polyurethane, and Epoxies. Thermoset materials are hard, rigid, highly stable, resistant to high temperatures, and can be reinforced with strong fibres such as Kevlar or carbon fibre [38]. Furthermore, thermoplastics are considered a recyclable material. There are generally three methods for recycling thermoplastics: mechanical (crushing, cutting, or grinding), chemical (pyrolysis/gasification, depolymerization, dissolution), incineration (burned for combustion energy) [39], the last method is considered only if the material cannot be reutilized. PETG is a thermoplastic that can be recycled chemically by breaking the polymer chains back to their original components and reused as raw materials for new products [32]. Most recycling centres accept PET and high-density polyethylene (HDPE), However, not all recycling facilities accept PETG. The recycling procedure of PETG has to be conscious, for it is easily mistaken for PET. If tossed into the same recycling stream as PET, it will give the mixed material a lower melting point and change its out-of-spec thermal stability, hence, the entire mixed waste would be thrown into the incineration pile [40]. Though PETG can be more challenging than other type 1 materials to recycle, it is still one of the easiest thermoplastics to recycle [41]. Given the right recycling programs and facilities, as well as conscious of the waste that is discarded, recycling and remanufacturing remain relevant and important to our ecosystems and well-being.

2.4 Applications of 3D printing PETG

As mentioned in section 2.1, PETG is a thermoplastic that is derived from a petroleum-based source [42]. PETG is a versatile and durable material commonly used in industries for food packaging, medical devices, and signage. PETG filament is commonly used as a material for electronic devices for houses and light piping due to its durability, heat resistance, and minimal light scattering. In addition, PETG is biocompatible, and a large number of medical devices where sterilization is of high importance, for instance, surgical equipment, diagnostic equipment and drug delivery devices are manufactured from PETG due to its good chemical resistance [43]. Moreover, due to the simplicity of being able to colour PETG, it is often used to create retail stands and displays for marketing, PETG is more durable than acrylic as well as more formable than polycarbonate which makes it a popular choice for the manufacturing of machine guards [32]. The application of 3D printed PETG products have few constraints (brittle if not stored correctly, prone to oozing) [44]. Thus, the optimization and characterization of mechanical properties such as creep are essential for understanding the future capabilities of this material.

2.5 3D Printing parameters

2.5.1 Infill Density

The infill density is defined as the amount of material used to fill-in a part of a 3D printed object that is generally expressed as a percentage between 5-100 (%). The higher percent infill, the fuller, heavier, and in part, stronger the specimen is. Furthermore, infill density largely effects the amount of material needed to finish a part and the time it takes to print. Depending on the design of the part being printed, different infill densities are necessary. A lower density is used for a more flexible part, a higher density (70-100%) provides a more rigid part [45]. Ambati studied the effects of infill density and infill geometry on the mechanical properties of 3D printed PLA parts, and found that with almost all specimens, the tensile strength improved by margins when increasing the infill density from 60%, 75% to 90% [46].

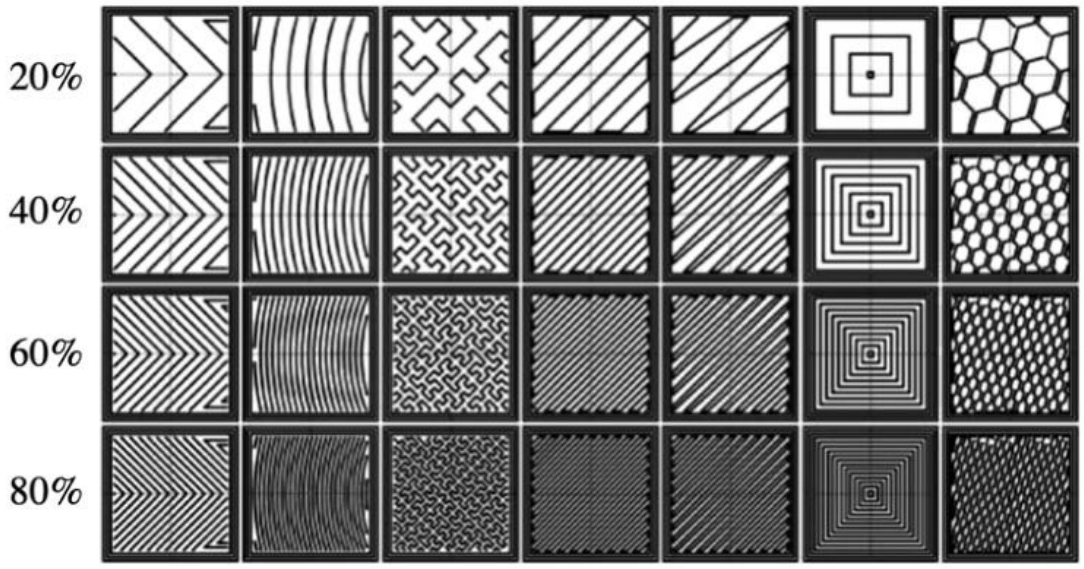

Figure 2 Common infill geometries and their densities [47] p. 13

2.5.2 Infill Orientation

Infill orientation can heavily manipulate mechanical properties such as tensile modulus and modulus of toughness [15]. Infill orientation is the printed direction of the internal layers of the specimen with respect to the longitudinal axis of the

sample [48]. Infill orientation tends to yield the strongest tensile properties when the load is orientated along the load direction (0 or 90°) this, is due to the longitudinal load distribution that the infill provides [49]. Mohammad Investigated the effects of build direction and unidirectional raster orientation on the creep response of 3D-printed PLA samples. The analysis concluded that specimens printed on its edge with a 90° infill orientation has higher yield stress while experiencing lower creep strength than those specimens printed on their surface with 90° infill orientation. Moreover, both samples that were printed on their surface and edge with a direction of 90° experienced better yield strength than the specimens printed on their surface and on their edge but with infill orientation of 0° [50].

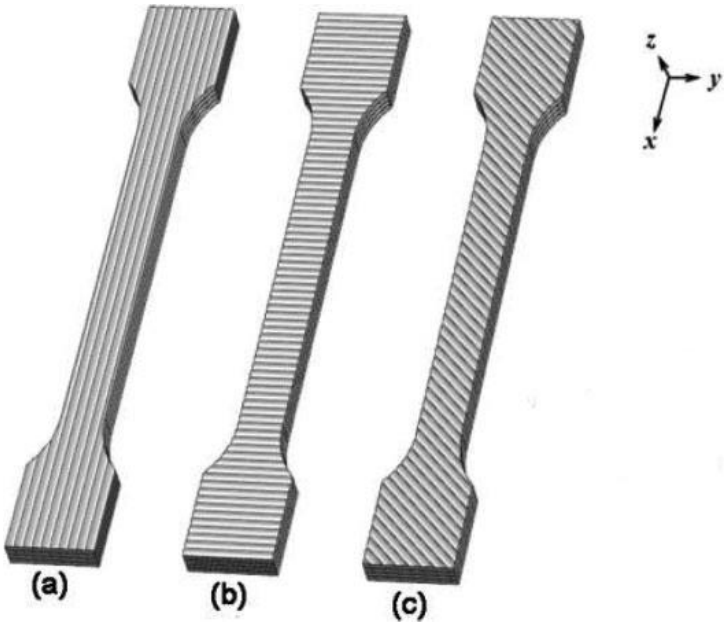

Figure 3 Illustration of print orientations (a=90, b= 0 and c= ±45) p.14 [51]

2.5.3 Infill Geometry

Infill geometry is the shape and formation of the internal structure of the printed part [52]. Dozens of infill geometries are available in most slicing software, including honeycomb, tri hexagonal, cubic, zigzag, and Gyroid to name a few. A brief description will be given of the infill geometries used in this study. Gyroid geometry, concaving irregular curvatures that overlap, the optimal balance between material usage, print time, and strength, it is one of the strongest geometries that can be printed. Cubic geometry stacked cubic formations tilted by 45° around the X, and Y-

axes which provides good strength in X, Y, and Z directions. However, requires more material than most other geometries. Tri hexagonal geometry, lines crossing and overlapping in X, Y by producing hexagonal patterns with triangles located in between and provides excellent strength in two directions. [53]

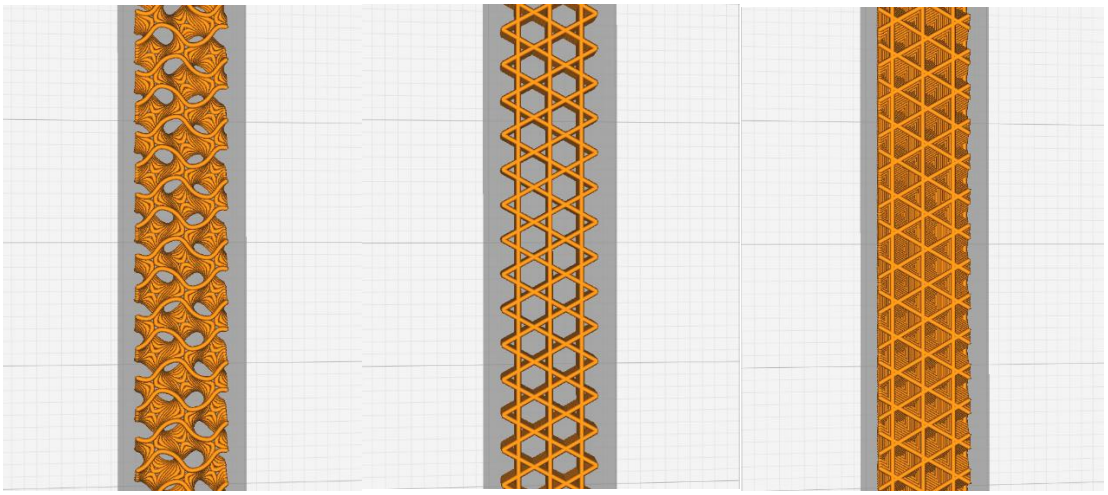

Figure 4 Gyroid p. 15 *Figure 5 tri hexagonal p. 15* *Figure 6 cubic p. 15*

The image above illustrates the infill geometries used in this thesis.

2.5.4 Nozzle temperature

The nozzle temperature describes the temperature of the 3D printer's nozzle in where the molten filament is extruded. The printing temperature is usually between $180°C$ - $260°C$ (enough heat to melt the filament) it is dependent on the makeup of the polymer filament; the temperature usually lies above the glass transition temperature but below the melting point. The glass transition temperature is different for each material, it expresses the transition state where the material turns from a brittle state into a rubber state, which usually happens with amorphous materials, this is a reversible transition [54]. Furthermore, nozzle temperature can affect the mechanical strength depending on the molecular state of the material. A study by Morteza describes how the nozzle temperature affects polylactic acid (PLA) a semi-crystalline material. His research showed that the higher processing temperature of PLA (260 C°) gave a higher tensile modulus [55]. This could be due to the high processing temperature of the polymer. The longer the polymer has time to cool, the higher the crystallinity hence, increasing its mechanical strength [56]. The printing temperature is important, if too high temperature, there is a higher risk

of damaging the material due to thermal degradation. Moreover, high temperatures of above or equal to its melting point, can produce difficulties when printing due to the viscosity of the polymer. PETG has a printing range between $220°C$ - $250°C$, with a print bed temperature of $50°C$ - $80°C$. The print bed temperature is the temperature of the plate on which the 3D part will be printed. The print bed allows slower cooling rates and is important for restricting shrinkage and warpage of the part during the duration of the print. [57]

2.6 Creep

Creep is the irreversible deformation of a material over a length of time, in the presence of a constant load. Creep is affected by variables: stress, strain and time. Creep can be noticed in all crystalline materials including metals and glass [58]. The analysis of creep is essential for determining the possible long-term failures caused by high stresses and constant loads, for example, bolts loosening due to relaxation and pre-stressing or jet engine turbine motors failing due to increased temperatures and rotational stresses. [59] [60]

2.6.1 Stages of Creep

Creep is divided into three separate stages: primary creep, secondary creep, and tertiary creep. Primary creep is associated with the instantaneous deformation of the material, in this stage, the creep rate $(\dot{\epsilon})$ is infinite where $-1s < m < 0s$ in which m is the time index, meaning the time under a tensile load. Following primary creep, is secondary creep, where $m = 0s$, this stage normally lasts the longest and is where the strain rate remains constant. The last stage of creep, tertiary creep, is where the strain rate starts to grow rapidly due to internal stress and increased strain rates. In the final stage, the strain rate continues to increase rapidly until a fracture occurs. [60]

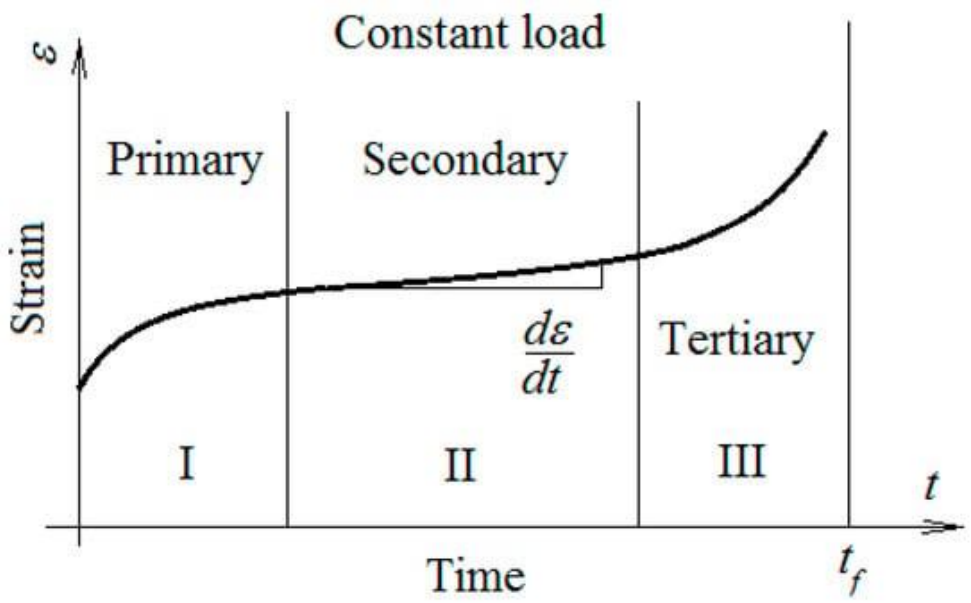

Figure 7 Standard plot displaying Primary, Secondary and Tertiary creep [61]

Normal (linear) strain: The instantaneous deformation

$$\varepsilon = \frac{\Delta L}{L_0} \quad (1)$$

$$Initial\ strain\ = \frac{final\ length - original\ lenght}{original\ length} \quad (2)$$

Strain rate: The change in strain with respect to time

$\dot{\epsilon}$ Strain rate

$d\varepsilon$ Change in strain

dt Change in time

$\dot{\epsilon} = \frac{d\epsilon}{dt}$ [62]

2.6.2 Creep Modulus

In material creep, small deformation under time is usually desired. Creep Modulus (MOC) unite is represented by MPa, and a higher value is equivalent to a tougher material and less deformation over time. Thus, a low MOC is equal to a weaker material, and not sought after for good creep behaviour. Creep modulus is taken from an individual time point or interval depending on what is being studied.

$$MOC = \frac{\sigma}{\epsilon_c} \qquad 3$$

Creep modulus is equivalent to the value of stress divided by the value of strain after a given time [63]. Creep modulus is a good way to represent the creep of a material numerically and can be plotted against time to see how the creep changes under a period.

2.7 The Taguchi method

Dr. Genichi Taguchi, a statistician and engineer in the early 1950s, developed a methodology for improving quality control of manufactured goods whilst reducing costs [64]. The method known as "The Taguchi method" [65]involves reducing the variation of a process. Through a robust design of experiment (DOE) approach, Dr. Genichi developed a system that investigates how different parameters of a process effect the variance and mean of the performance variables that define how well a process is functioning. Taguchi's DOE provides an accurate and efficient method of understanding the relationship between process parameters and optimization. D. Lestari applied the Taguchi method for the optimization of printing time and socket weight of 3D printed socket prosthetic manufacturing. Following the DOE, Lestari concluded that the factors which contributed to a better signal-to-noise ratio were, layer height of 0.2 mm, print speed of 80 mm/s, infill density of 100 %, and thickness of 3 mm with nozzle temperature of 180 $°C$ [66]. In addition, Wicaksono applied the Taguchi method to improve the dimensional precision of 3D-printed PLA

ring-shaped specimens. Wicaksono concluded that the best printing parameters that result in optimal dimensional accuracy are layer height of 0.25mm, printing speed 20 mm/s, ambient temperature of 34 °C, infill percentage of 40 %, bed temperature of 62 °C and nozzle temperature of 200 °C [67].

The method of Taguchi's DOE involves the creation of an orthogonal array, the size of the array is defined by the number of parameters and factors being analysed. Each element in the array represents a level of a factor, each level represents a variable of a process for example, factor: infill density (Level: 20%, 50%, 80%), factor: infill geometry (Level: Zigzag, Cubic, Gyroid, Tri hexagonal). Unlike a full factorial design, where there is need to test every variable independently. The Taguchi approach tests pairs of combinations with other sets of pairs and determines the number of interactions between each set of pairs, thus measuring the fewer the interactions between pairs and groups of pairs, the less significant the variable has on its factor.

The design of experiment is made by creating an orthogonal array and give each factor and their level a position in the array, afterwards the experimental testing can be carried out. After the experiments have been conducted, analyses of the data to determine the effect that each level has on its output is calculated. The signal-to-noise ratio is calculated for every experimental run [68]. Signal-to-noise ratio (SNR) is a quality criteria and is defined as the relationship between the desired output of a signal and the undesired output of the signal, for example background noise e.g. factors that affect the results of an analysis that are not part of the experiment [69]. Furthermore, optimization of the parameters can be done with the data collected from the Taguchi DOE through analysis of variance (ANOVA) and further plotted, for better visual analysis.

SN number:

$$SN_i = 10\ log \frac{\bar{y}_i^2}{s_i^2} \qquad 4$$

Mean value:

$$\bar{y}_i = \frac{1}{N_i}\sum_{u=0}^{N_i} y_i, u \quad (5)$$

Variance:

$$s_i^2 = \frac{1}{N_{i-1}}\sum_{u=0}^{N_i}(y_i, u - \bar{y}_i) \quad (6)$$

were

$\boldsymbol{i}$ Experimental Number

$\boldsymbol{u}$ Trial number

$\boldsymbol{N_i}$ Number of trials for the experiment $\boldsymbol{i}$

The data analyses conducted in this thesis are the output responses of multiple creep experiments. In most creep experiments, the desired outcome is low creep behaviour. Thus, in the case of minimizing the output response, the following definition of the SN ratio should be utilized. [68]

Minimizing SN ratio/the smaller the better:

$$SN_i = -10log\left(\sum_{u=1}^{N_i}\frac{y_u^2}{N_i}\right)$$

After calculating each SN ratio, the average SN ratio is calculated for every factor and level to find the ranking of most to least significant [68]. A significant ranking of e.g., 1 is considered to be the strongest of the 9 samples, meaning harder to deform.

Table 1 Example of SN ratios and their groups p. 21

Experimental number	P1	P2	P3	P4	SN
Run 1	1	1	1	1	SN_1
Run 2	1	2	2	2	SN_2
Run 3	1	3	3	3	SN_3
Run 4	2	1	2	3	SN_4
Run 5	2	2	3	1	SN_5
Run 6	2	3	1	2	SN_6
Run 7	3	1	3	2	SN_7
Run 8	3	2	1	3	SN_8
Run 9	3	3	2	1	SN_9

$$SN_{P3,1} = \frac{(SN_1 + SN_6 + SN_8)}{3}$$

$$SN_{P3,2} = \frac{(SN_2 + SN_4 + SN_9)}{3}$$

$$SN_{P3,3} = \frac{(SN_3 + SN_5 + SN_7)}{3}$$

$$\Delta = Max - Min$$

Table 2 Example calculation of Delta and ranking of factors p. 22

Level	Factors			
	P1	**P2**	**P3**	**P4**
1	$SN_{P1,1}$	$SN_{P2,1}$	$SN_{P3,1}$	$SN_{P4,1}$
2	$SN_{P1,2}$	$SN_{P2,2}$	$SN_{P3,2}$	$SN_{P4,2}$
3	$SN_{P1,3}$	$SN_{P2,3}$	$SN_{P3,3}$	$SN_{P4,3}$
Delta (Δ)	Rp_1	Rp_2	Rp_3	Rp_4
Rank	…	…	…	…

2.8 Analysis of Variance (ANOVA)

ANOVA tests are carried out for understanding if there exists a relationship between more than two groups concurrently. ANOVA categorizes a data set into 2 categories (systematic factors and random factors). Systematic factors are factors of a data set that affect the response output. Random factors are factors that don't affect the response output. [70]

The results of an ANOVA provide an F-statistic and F-ratio. If the F-ratios value is close to 1, the differences between the groups are very little or non-existent. When there are no noticeable observations between groups, this is called a null hypothesis. [71] A. Hassan carried out an ANOVA analysis on friction stir welding (FSW) parameters and found that the parameters that had the highest effect on the tensile strength and hardness was the transverse welding speed, and second most important parameter was rotational speed [72]. Furthermore, Atefeh R. applied Taguchi DOE and ANOVA to optimize properties for 3D printed PLA. Atefeh R. concluded that there were heavy correlations between groups and found the optimum input parameters for tensile strength and toughness were Infill density (60%), extrusion temperature (200 °C), raster angle (-45/45°) with layer thickness (0.2mm) [73].

2.8.1 Sum of Squares and ANOVA Table

Total sum of squares and Correction factor

Total sum of squares (SST) measures the total variation of the response data. SST shows the total observed variation of the data about the mean. The sum of square helps us to understand the differences between groups. [70]

$$SS_T = SS_f + SS_e$$

Furthermore, the SST can be given by subtracting a correction factor (CF). Correction factor is used for simplifying the sum of squares computation it is a constant that eliminates the effect of the grand mean which leads to more accurate ANOVA results and shows the true variation of the group and error data.

$$CF = \frac{Y_{..}^{2}}{N} \quad 7$$

$$SS_T = \sum_{i=1}^{m} \sum_{j=1}^{n} Y_{ij}^{2} - CF \quad 8$$

N = Total number of observations

Y = All experimental observations

Below is an example of computing the total sum of square of multiple factors using CF factor.

$$SS_T = \sum_{i=1}^{a} \sum_{j=1}^{b} \sum_{k}^{c} \sum_{l}^{n} Y_{ijkl}^{2} - CF \quad 9$$

SS for a single factor with n levels

$$SS_A = \frac{\sum_{i=1}^{a} Y_i^{2}}{bcn} - CF \quad 10$$

b = Number of levels of factor B

c = Number of levels of factor C

n = Number of experimental repetitions

Sum of squares of error

The sum of square of error (SSE) represents the outliers of the data, meaning the data that cannot be explained by the model e.g., random error, residual variation. The sum of square of the error is computed by subtracting the SS_T and the SS of each factor as well as the interaction between each group SS_{ABC}. In this research, no interactions are considered, only the main effect.

Equation 11

$$SSE = SS_T - SS_A - SS_B - SS_C - (Interactions\ betwen\ groups)$$

3. Method

3.1 Specimen design and printing parameters

3.1.1 Dimensions

The specimens are designed as tensile test specimens and follows the standard ISO 527-2 [1A]. The specimens are constructed by 3D computer aided design software (CAD). CAD software is used in all areas of engineering and architecture for designing of tools and equipment outdoor and indoor installations, optimization of products and the CAD software is very versatile [74]. The software-SolidWorks 3D - CAD was utilized for modelling of the samples [75].

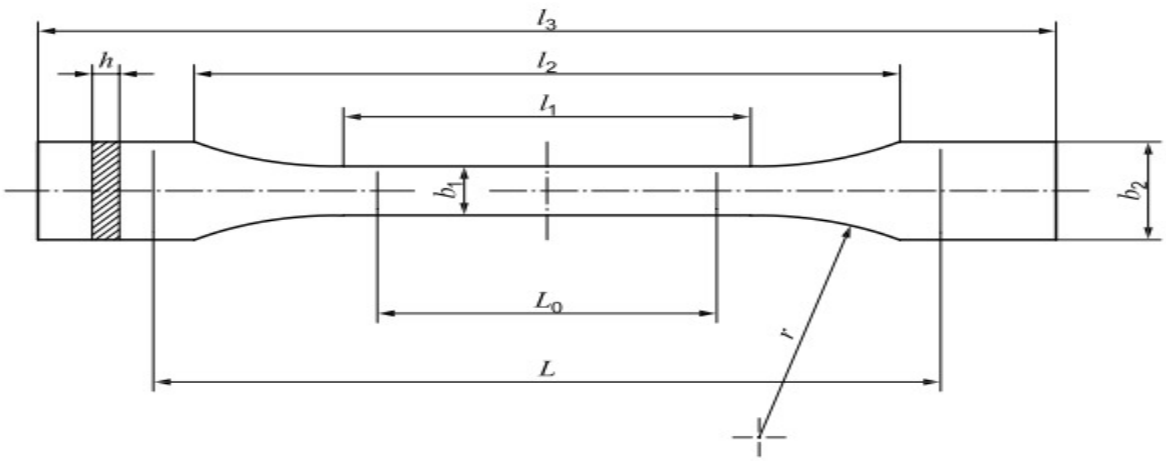

Figure 1 — Type 1A and 1B test specimens

Figure 8. Tensile dog bone STANDARD ISO 527-2 [1A]/[1B] p. 25

Table 3 Dimensions of dog bone specimen p. 25

	Specimen type	**1A (mm)**
l_3	Overall length	170
l_1	Length of narrow parallel-sided portion	80±2
r	Radius	24±1
l_2	Distance between broad parallel-sided portions	109.3±3.2
b_2	Width at ends	20±0.2
b_1	Width at narrow part	10±0.2
h	Preferred thickness	4±0.2
L_0	Gauge length	75±0.5
L	Initial distance between clamping grips	115±0.5

3.1.2 Slicing

After modelling the tensile test specimens, the SolidWorks file (.STL) is exported and then imported into a 3D slicing software called Ultimakers Cura, which is the same slicing software used for defining the print settings. Once the 3D model has been uploaded into Cura, Cura slices the part, meaning it translates the model into G-code which the 3D printer can later compute.

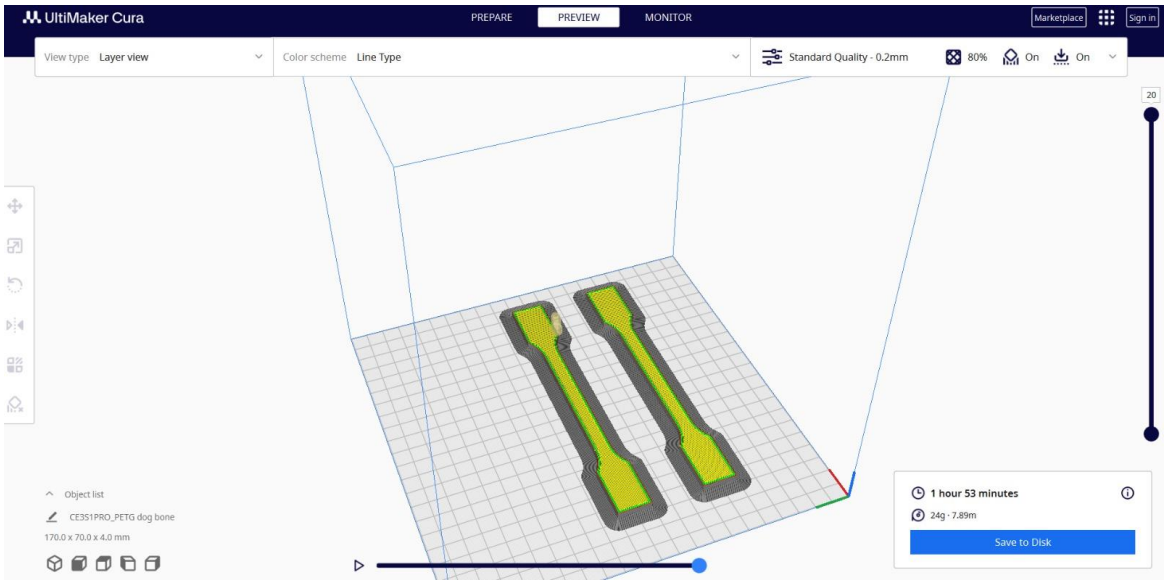

Figure 9. UltiMaker Cura slicing software p. 26

3.1.3 Printing

Ender-3 S1 Pro printer was utilized for the printing of the samples. In total, the print time for 14 samples took roughly 15 hours. Furthermore, 12-24 grams of PETG material was used for each pair of samples, depending on the infill density and a geometry equivalent to 3-7.5 meters of filament. Approximately 1-2g of material waste for every printed part. The waste is due to the added brim layer on the surface of the print bed. The brim layers, also known as skirts, are additional printed outlines around your modelled part. The skirt helps hold edges of the modelled part down, helps with print bed adhesion, and can prevent warping of the specimen [76].

3.2 Experimental method

The design of experiment applied in this research follows Taguchi's L_9 orthogonal array consisting of four three-level factors, each given a position in the array (table 5.). The factors are infill density, orientation, geometry, and nozzle temperature. The factor levels are represented by integers between 1-3 (table 4.).

Table 4 Level notation for factors p.27

	Factors			
level notation	Infill geometry	Infill orientation°	Infill Density %	Nozzle temperature C°
1	Tri-hexagonal → 1	90 → 1	80 → 1	250 → 1
2	Gyroid → 2	45 → 2	50 → 2	235 → 2
3	Cubic → 3	0 → 3	20 → 3	220 → 3

Table 5 L_9 orthogonal array including factors and experimental runs p.27

	Factors			
Experimental run	Infill geometry	Infill orientation	Infill density	Nozzle temperature
		L9 orthogonal array		
1	1	1	1	1
2	1	2	2	2
3	1	3	3	3
4	2	1	2	3
5	2	2	3	1
6	2	3	1	2
7	3	1	3	2
8	3	2	1	3
9	3	3	2	1

The L_9 array is based on a $3\ x\ 4$ factor level. Hence, a 3-level fractional factorial design is used. In this experimental approach, we are concerned only with the impact of each factor, for this reason, only the main effects are considered, resulting in 8 degrees of freedom (DOF). The DOF is done in statistical analysis calculations like a one-way ANOVA. For clarification, DOF is equivalent to the number of factor levels observed minus the number of constraints observed [77], for each $DoF = number\ of\ levels - 1 = 3 - 1 = 2; tot\ DoF = 2\ x\ 4 = 8.$

3.3 Material and sample testing

The PETG acquired for the experimental analyses and sampling was ordered from a Polish fused feedstock deposition (FFD) manufacturing company known as Devils Design Products. The package contained artificial PETG filament, vacuum-packed on a reel which included a humidity absorber to not absorb any excess water during transport and storage [78]. The same PETG was used for both creep testing and tensile benchmarking. To start the experimental testing, the correct factorial design must be chosen. Once the design of experiment has been decided on, sample manufacturing can proceed. The printing of the samples was carried out utilizing an Ultimaker S3 FFF 3D printer [79]. Following sample manufacturing, a quasi-static tensile test was conducted. A total of 13 samples were tested, 4 of which were used for benchmarking and no additional repetitions were carried out. As mentioned, samples are designed per the ISO 527-2 [1A]:2012 standard. To summarize DOE selection, sample manufacturing, testing and analyses approach can be seen below.

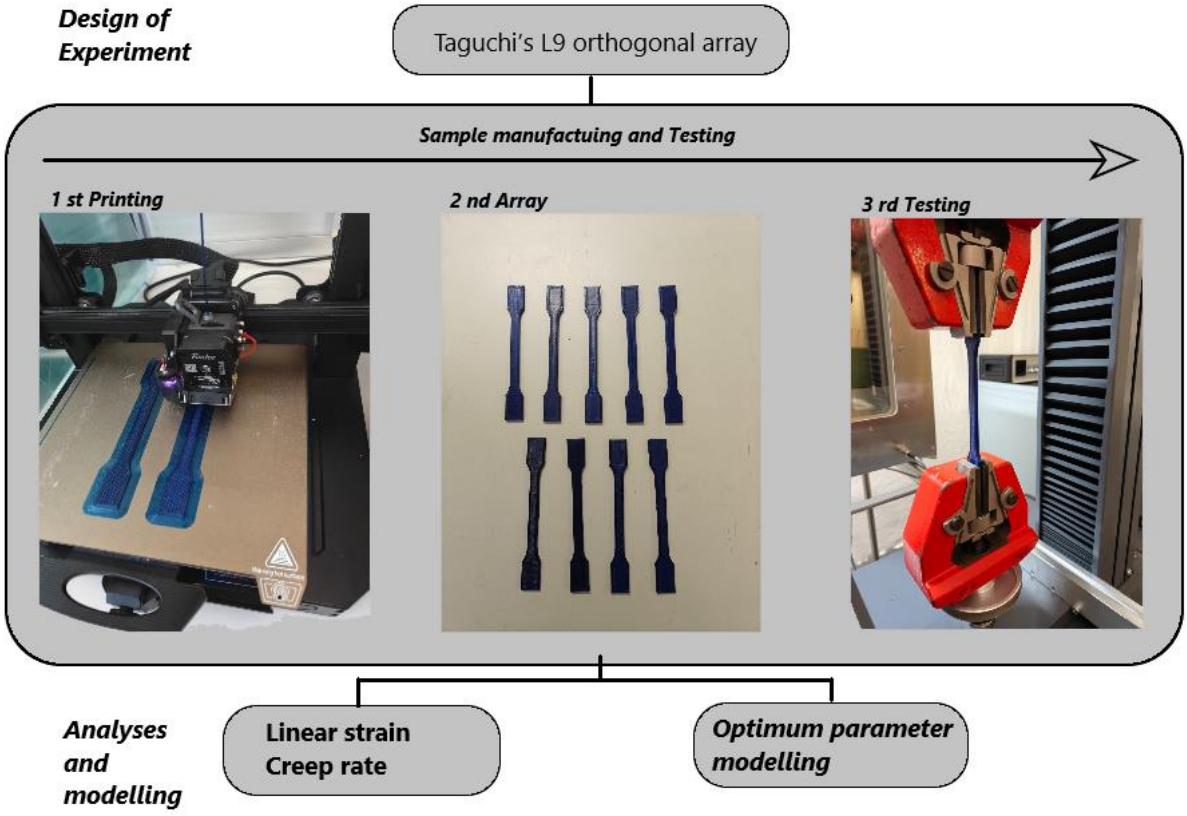

Figure 10. Summarization of DOE, sample manufacturing/Testing and Analyses p.28

3.3.1 Benchmarking

Considering that a creep test is a slow static tension test, we don't want instantaneous fracture to occur for the specimen. Thus, a standard tensile benchmark test was conducted for a frame of reference, and for defining the desired force required to produce deformation but yield before any fracture or breakage. Fracture of the tensile specimen occurred just after 3 % strain at a stress of 37 MPa. Moreover, the tensile specimen tested was sample 1, which was hypothesized to be one of the strongest of the samples, due to its high infill density, infill orientation (in load direction) and strong geometry (table 5.). From the results we can derive a stress value that is suitable for conducting creep analysis.

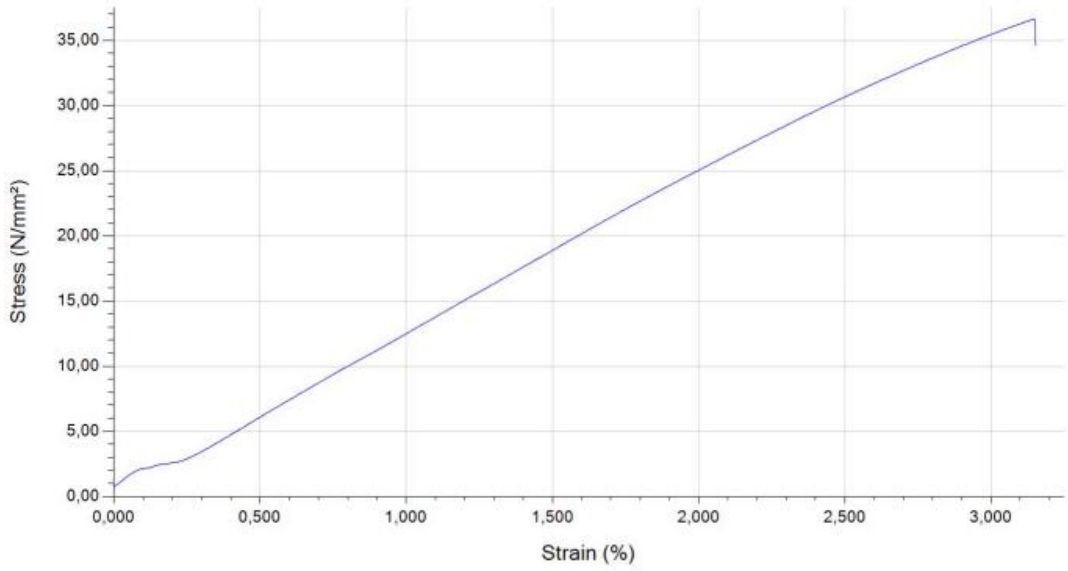

Figure 11. Tensile benchmark test: Sample 1 p.29

A stress value of 15 MPa is considered a good force for conducting the creep tests which is situated at about halfway point to rupture. However, after consideration, it was decided upon to be certain that the force chosen is suitable for most specimens, before testing begins, to test the 15 MPa on the presumed strongest and weakest test specimens; sample 1 and sample 3. Sample 3 is one of the weakest samples due to low infill density of 20 % and infill orientation of 0° (perpendicular to load direction.).

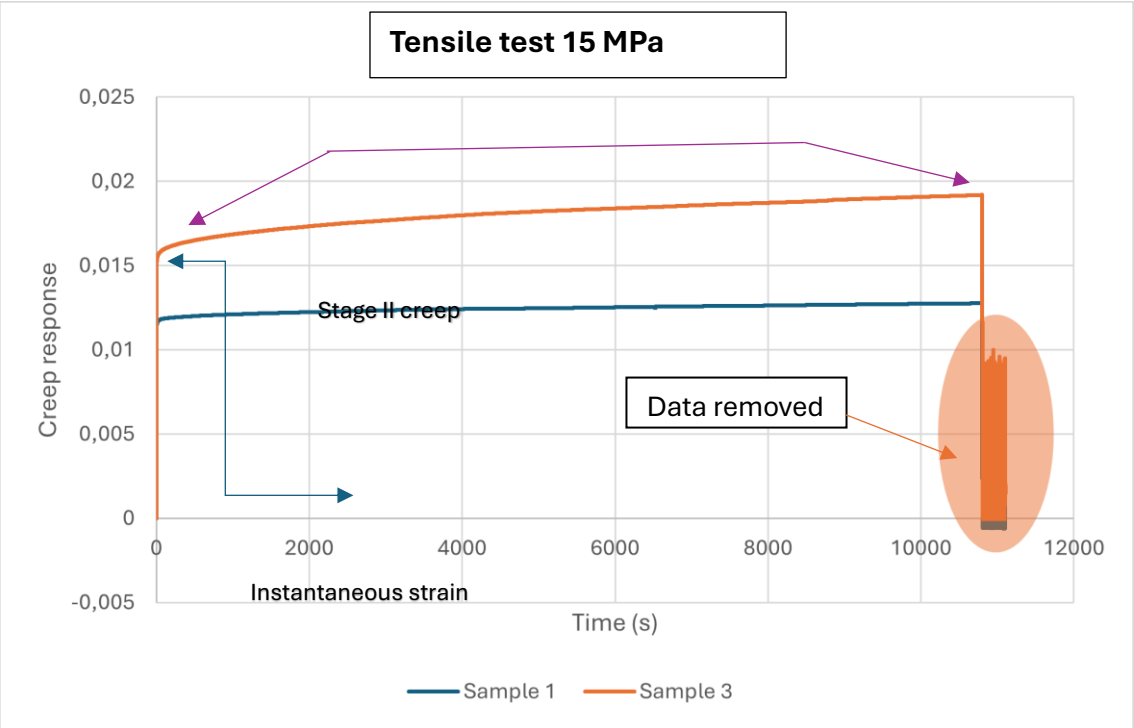

Figure 12 Tensile tes test on strongest and weakest samples. *p.30*

Studying the strain response of samples 1 and 3, notice how the Initial (instantaneous) strain response differs from sample 1 to sample 3. Sample 1 experiences an initial strain of 0.011 (1.1 %) and sample 3 an initial strain of 0.0152 (1.52 %). There are noticeable differences between the instantaneous strains of both samples. However, no fracture occurred. Studying both samples, the strain rate in stage II creep for sample 1 remains more constant than that of sample 2. This indicates that the applied force of 15 MPa for studying the creep behaviour is too low of a force for some stronger samples that will be tested. To extract more valuable and relevant data from our experiments, another 5 MPa was added to the applied load. Meaning a 20 MPa load will be used for the creep testing.

3.3.2 Creep testing

Determination of creep behaviour follows ISO 899-1:2017, each experimental run was conducted by applying a load of 20 MPa force acquired from the tensile benchmark. Furthermore, time-dependent deformation was studied during each test run. The time for every experimental run was approximately 10 800 seconds (3 hours) held at a 20 MPa with a test speed of 5 mm/min. In the last 5 minutes of each

experimental run, the force decreased from 20 MPa to 0 MPa. We are only interested in the creep data. Hence, the last 5 minutes of data will be subtracted from the data set. The last 5 minutes is the distressing state of the tensile test machine (figure 9.) in which, the tensile machine removes the load and finds an equilibrium state to further remove the specimen from the machine safely.

4. Results

4.2 Visual analysis after testing

After testing, visual analysis is done and the samples are studied for deformations cause by the mechanical testing. Figure 10 illustrates the 9 samples after they have been tested. Each sample exhibited no fracture under the entirety of the tensile test (excluding benchmark samples). Visually it is difficult to see the longitudinal deformation of the specimens, however, the surface properties, such as, surface roughness and the quality that lay near the surface, can be seen to have experienced damage during the testing.

Figure 13. Tensile specimens after creep tests p.31

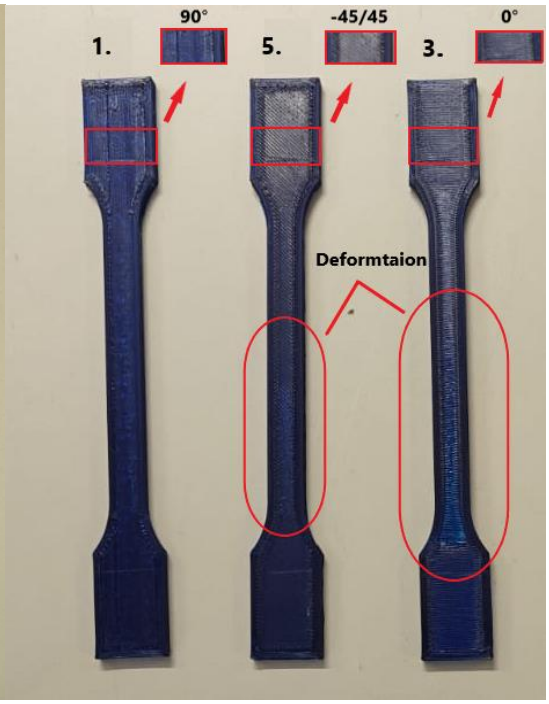

Figure 14. Samples 1,5 & 3, Infill orientation and deformations p.31

Figure. 11 include samples 1, 5, and 3, infill orientations (90°, -45/45° and 0°), infill density (80%, 50% and 20%) respectively, ordered from left to right. The figure is provided for representing the deformation that can occur for different infill orientations and densities. Ignoring the clamping damage done near the ends of the tensile test specimens, sample 1 has experience very little damage due to its high density and infill orientation (90 degrees) that lay along the narrow centre (gauge).

The surface quality remains intact, with no visual marks of elongation or breakage. Moreover, sample 5, with 50% density, with infill orientated at -45/45° shows slightly more regarding surface damage. Below the centre point of sample 5, it is a slightly brighter colour from the lower clamping section, it starts off blue then turns slightly brighter at the centre, and near the top, it returns its colour.

The gauge of the dog bone is meant for studying the material properties while it undergoes mechanical testing it is in this section, if fracture occurs it is most likely to be, if not desired to be. The bright blue is due to stress concentration points near the centre. At the stress centres, there is noticeable surface damage, however, the damage overall is very localized. Sample 3, with infill orientation perpendicular to the load direction (0°) has experienced much of the damage. Sample 3 has deformation from the lower clamping area to the upper clamping area. The damage, like sample 5, begins near the lower section (shoulder) of the specimen and travels upwards along the length of the gauge. Most of the damage is localized near the lower shoulder of the specimen. Localized deformation near the shoulders of the specimen often indicates a poor stress distribution this can be due to localized defects (high porosity or voids), dimensional errors, or human error when installing the specimen for analysis.

4.3 Creep response

The figure below represents the creep response for samples 1, 7 and 4. Each sample with an infill orientation of 90 °. Furthermore, sample 1 printed with 80 % infill density, tri hexagonal infill geometry and with nozzle temperature of 250 °C. Sample 4 printed with 50 % infill density, gyroid infill geometry and with nozzle temperature of 220 °C. Lastly, sample 7 printed with 20 % infill density, cubic infill geometry with nozzle temperature of 235 °C.

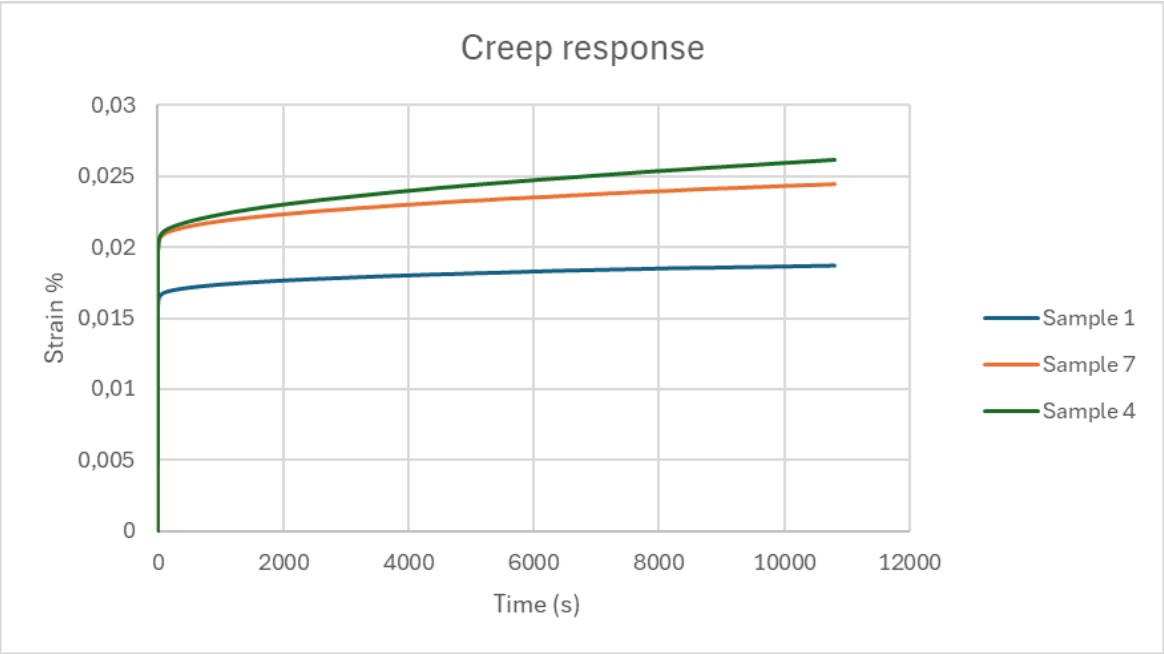

Figure 15 Creep response for samples 1, 7, and 4 all with 90 degrees infill orientation p.33

Figure 12 represents the creep response for samples 6, 9 and 3. Each sample with infill orientation of 0 °. Sample 6 printed with 80% infill density, gyroid infill geometry, and with nozzle temperature of 235 °C. Sample 9 printed with 50% infill density, cubic infill geometry, and with nozzle temperature 250 °C. Lastly, sample 3 printed with 20% infill density, tri-hexagonal infill pattern and with nozzle temperature of 220 °C.

Figure 16 Creep response for samples 6, 9 and 3 all with 0 degrees infill orientation p.33

The final graph below displays the creep response for samples 8, 2 and 5. Each sample with print orientation of -45/45 °. Sample 8— printed with 80% infill density, cubic infill geometry, with nozzle temperature of 220 °C. Sample 2 printed with 50% infill density, tri-hexagonal infill geometry, and with nozzle temperature 235 °C. Sample 5 printed with 20% infill density, gyroid infill geometry and with nozzle temperature of 250 °C.

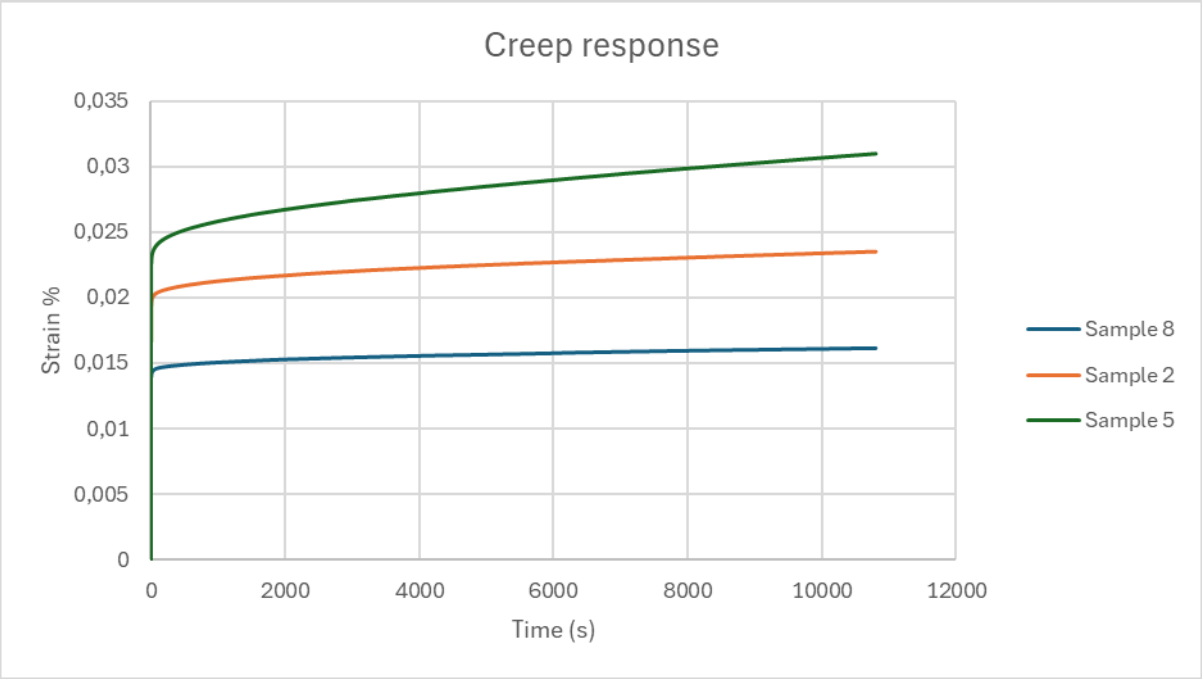

Figure 17 Creep response for samples 8, 2 and 5each with infill orientation -45/45 p.34

4.4 Creep modulus

Another way of graphically representing creep, is by plotting the creep modulus over time. Figure 14-15 shows the MOC of all the samples with MOC on the y-axis and time represented on the x-axis. When analysing MOC a higher value describes stronger resistance to deformation.

Figure 14 MOC of samples 4, 5, 7 and 9 p.35

Figure 15 MOC of samples 3,1,8,6 and 2 p.35

5. Discussion

Table 6 shows the comparison of creep modules for all samples. The samples are ranked as strongest to weakest, with the factor level included for seeing the relationship between factor, factor level and experimental outcome. Furthermore, the average of the creep modulus is presented below.

Table 6 Creep modulus ranked p.36

Sample	MOC (MPa)	Infill Density %	Infill Geometry	Nozzle Temperature $°C$	Infill Orientation °	Rank Order
8	1270,89	80	Cubic	220	45/-45	1
6	1160,91	80	Gyroid	235	0	2
1	1096,44	80	Tri-Hexagonal	250	90	3
9	898,46	50	Cubic	250	0	4
2	883,77	50	Gyroid	235	45/-45	5
7	853,03	20	Cubic	235	90	6
4	812,25	50	Tri-Hexagonal	220	90	7
3	711,54	20	Tri-Hexagonal	220	0	8
5	693,64	20	Gyroid	250	45/-45	9

It is clearly noticeable from the above table that the creep modulus increases with infill density. The three samples with the highest creep modulus are samples 8, 6, and 1 all with 80% infill densities. Furthermore, the three samples with the lowest creep modules are samples 4, 3, and 5 with infill densities of 50%, 20% and 20% respectively. The creep modulus strengths are not only dependent on the infill density. The data above displays a picture of increasing creep modulus with increasing density. However, samples 7 and 4 are outliers in the data. Sample 7 has a 20% infill density with a creep modulus of 853,03 MPa, sample 4 has an infill density of 50% with a lower modulus of 812,25. This small difference is the cause of other leading factors, mainly infill geometry.

Infill geometry may not be the main factor determining the material's creep response, but it is secondary to infill density. By looking at the creep modulus and its equivalent sample geometry. There is a trend of cubic being the stronger pattern followed by gyroid and tri hexagonal.

The first three samples presented in the table, all with 80% infill density and have the infill geometry ordered as 1st cubic, 2nd gyroid, and 3rd tri hexagonal. The middle three samples are sample 9 with 50% infill density, sample 2 with 50% infill density, and sample 7 with 20% infill density. Samples 9, 2, and 7 have infill geometries ranking 1st cubic, 2nd gyroid, and 3rd cubic, respectively Just below sample 7 is sample 4 with 50% infill density with only a difference of 40.70 MPa.

Samples with infill density of 80% have a creep modulus between 1100-1300 MPa. Samples with infill density of 50% have a creep modulus between 800-900 MPa. Samples with infill density of 20% have a creep modulus between 700-850MPa. Infill density and infill geometry have relatively noticeable effects on the creep modulus. Moreover, the infill orientation and nozzle temperature have an almost random ordering, suggesting that factors, nozzle temperature and infill orientation do not have a significant effect on the creep response relative to the infill density and infill geometry.

Table 7 The SN ratios Smaller-the-better following creep modulus response

Test	Factors				SN ratio
	Infill geometry	Infill orientation	Infill density	Nozzle temperature	Creep
1	1	1	1	1	-6.7418
2	1	2	2	2	-8.6032
3	1	3	3	3	-10.438
4	2	1	2	3	-9.3083
5	2	2	3	1	-10.672
6	2	3	1	2	-6.2621
7	3	1	3	2	-8.9037
8	3	2	1	3	-5.4663
9	3	3	2	1	-8.4096

The Taguchi method, involved firstly, computing the signal-to-noise ratio (S/N) smaller-is-better seen in table 7. The analysis was done with the data from the creep experiments, starting from where the force was constant and excluding the last 5 minutes of the experiment. Figure 19 displays the four factors and levels with SN ratio presented on the y-axis displaying the optimum factor levels.

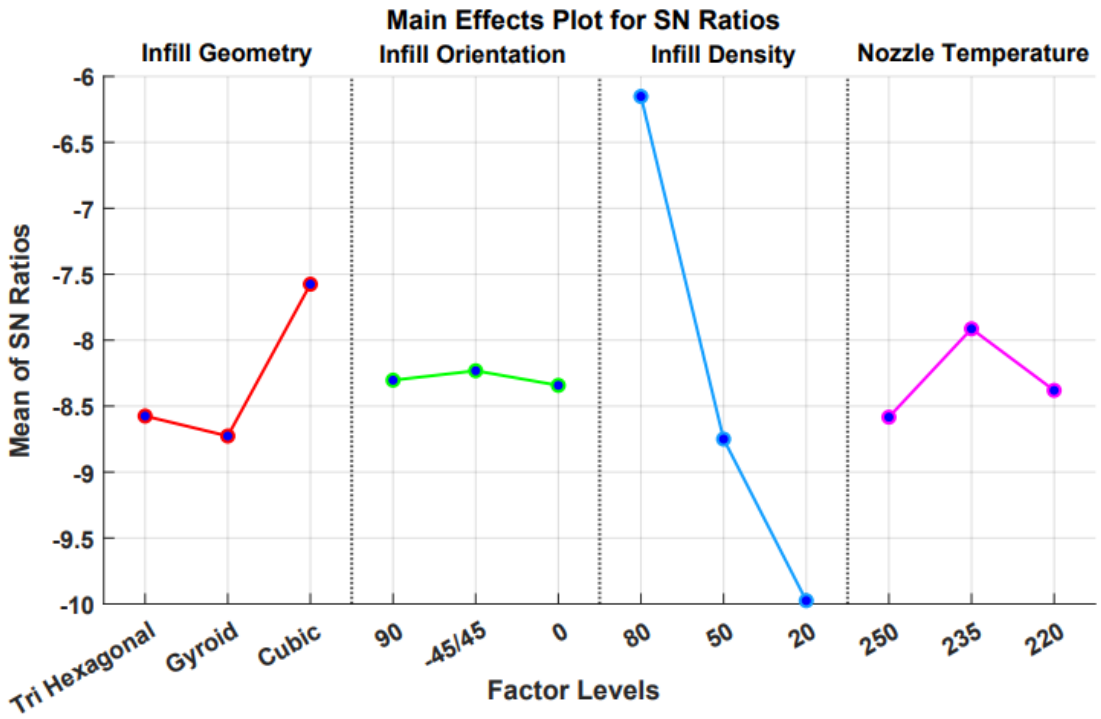

Figure 16 Optimum SN ratios for factor levels p.38

From Figure 19. The infill geometry shows an SN ratio of -8.55 for the tri hexagonal geometry, -8.75 for the gyroid geometry and a value of -7.55 for the cubic geometry. Considering the smaller signal is desired in this analysis (smaller, meaning closest value to 0) the cubic geometry shows slightly more desirable results than the others. However, the difference between the least significant infill pattern (gyroid) and the more significant infill pattern (cubic) is -1.2 which is a small variance. Gyroid and tri-hexagonal patterns lay roughly at the same SN ratio with a difference of about -0.2. Therefore, the gyroid and tri-hexagonal pattern can be considered as equal in significance.

The infill orientation denoted with a green line appears strongest with -45/45° degrees in the print direction with an SN ratio of -8.25. Print orientation of 90 degrees is second with an SN ratio of -8.3. This is surprising considering the direction of 90 degrees is along the force direction. Moreover, 0 degrees infill orientation is the lowest with an SN ratio of -8.34 this, however, is expected due to the fibers oriented perpendicular to the force vector. Infill orientation is the least significant factor, this could be due to the type of manufacturing. In 3D printing, the specimens are built layer-by-layer hence, increasing the chance for a weaker internal structure due to voids, and uneven layer adhesion especially in lower densities.

Table 8 SN Ratio response table for each factor level with corresponding factor rank p.39

Level	Factor			
	Infill geometry	**Infill orientation**	**Infill density**	**Nozzle temperature**
1	-8.594	-8.317	-6.156	-8.507
2	-8.747	-8.247	-8.773	-7.923
3	-7.593	-8.369	-10.004	-8.404
Delta (Δ)	1.154	0.122	3.847	0.584
Rank	**2**	**4**	**1**	**3**

From the data on creep modulus strength in table 6 the infill density was the leading factor for a better creep response. This is also proven by SN ratios (Table 8.). The SN ratio of infill density has the highest and lowest ratios showing that this factor has the highest variance, thus having the highest impact on the creep response. The infill density displays a better SN ratio of -6.15 with a density of 80%. The second-best infill density is 50% with an SN ratio of -8.77. The lowest SN ratio is -10 with 20% infill density these results were expected due to the previously mentioned studies [45] [46] showing that a higher infill density results in tougher more rigid material.

The last factor studied nozzle temperature shows an SN ratio of -7.9 with a temperature of 235 degrees. Temperatures of 250 degrees and 220 degrees are relatively similar, with a difference of only -0.1 like infill geometry but overall,

slightly less significant and can be seen by less variation between the highest and lowest SN values.

Figure 20 displays the % contribution that each factor has to the creep response. Figure 17 shows graphically and denotes with the same colors as figure 19 how much of an effect each factor has on the creep response of the material.

$$\%\ Contribution = \frac{SS_{Factor}}{SS_{Totoal}} * 100\%$$

[80]

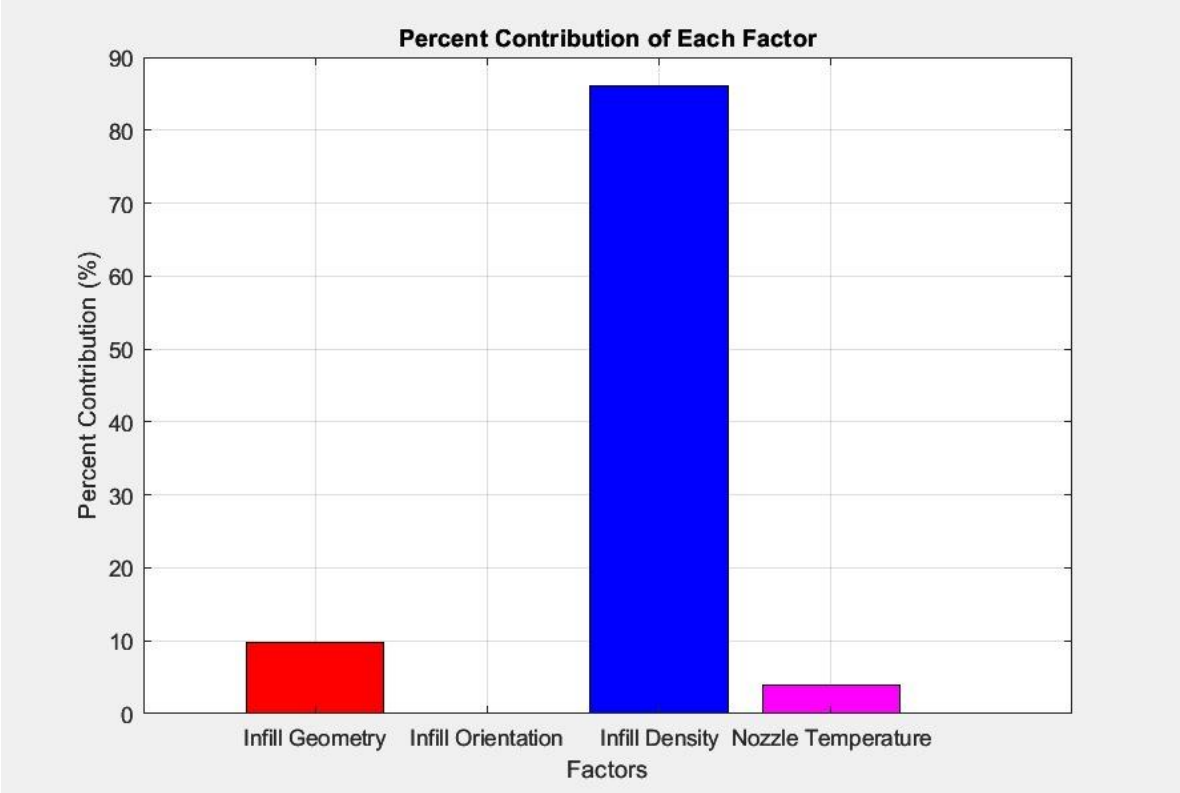

Figure 17 Percent contribution of each factor on the creep response p.40

The factor with the highest impact is highlighted in blue, infill density shows a percentage contribution of 85.69% this correlates with the creep modulus data as well as S/N ratios. An 85.69% contribution shows that the infill density has the highest impact on the creep response.

The second factor with a significant impact on the creep response is infill geometry highlighted in red infill geometry has a percent contribution of 9.73% with an almost ten times less of an impact than infill density.

The third significant factor is the nozzle temperature highlighted in pink with a % contribution of 4,47%. Such a low impact on the creep response can be considered as insignificant. However, it is largely the cooling rate of the material that determines the percent crystallinity which can cause the material to be either more elastic or more rigid [81]. Furthermore, the print bed temperature remained at a constant temperature of 80 degrees for all samples under printing. This temperature is quite high for a print bed. The difference between the lowest and highest nozzle temperatures does not create a big enough variation in cooling rate to notice any significant changes in the elasticity or rigidity of the material.

The factor with the least significant impact on the creep response is infill orientation. A contribution of 0.1% is insignificant and has little to no effect on the creep of the material. From previous studies [15] [49] infill orientation has always been the first or second contributing factor to the tensile strength of the material. However, those studies did not include such large % variation in densities, nor used such complex geometrical patterns for infill geometry. These two reasons alone can help explain the lack of an impact the infill orientation had. Furthermore, the sprinting of the specimens was done with almost max print speed of around 150 mm/s. Such high print speeds coupled with complex geometries could increase the number of structural defects and voids in between the layers and within the samples.

The ANOVA calculations require an error to term, the error term is used to account for the variation (noise) in the data it is needed for the calculation of the f-statistic and p-value. In the Taguchi design of experiment, there can be a lack of pure error due to DOE minimizing the number of experimental runs. The number of experimental runs in this thesis is 9 (with zero repetitions) thus leaving no room for error. In such cases, where the error term is infinitely small or zero, the least significant factor can be used as error if indeed the factor has a negligible effect on

the response output. Considering that the % contribution of the infill orientation is 0.1%, it can be considered to have a negligible effect on the creep response and will be used as the error term for the ANOVA.

The results from the four-way ANOVA studying only the main effects are displayed below.

Table 9 ANOVA table for Creep p.42

	Parameters						
Source of variation	Degrees of freedom (DF)	Sum of Squares (SS)	Mean square (MS)	F-Value	P-Value	% Contribution	Rank
A	2	1,54623E-05	7,73116E-06	97,978	0.0101	9,737	2
C	2	0,000136075	6,80377E-05	862,258	0.0011	85,69	1
D	2	7,10345E-06	3,55173E-06	45,011	0.0217	4,473	3
Error (B)	2	1,57813E-07	7,89063E-08				
Total	8	0,000158799					

The results from the four-way ANOVA indicate that infill geometry (factor A), infill density (factor C) and nozzle temperature (factor D) are all statistically significant with $\alpha = 0.05$ thus, the null hypothesis is rejected for all factors. Factor C has a ranking order of 1st with a % contribution of 85,69 % and p-value of 0.011. A low p-value indicates a larger impact on the creep response. Infill density has an f-value of 862.258 which is incredibly high for an f-value. A high f-value is due to the infill orientation which was used as the error term. Factor B (error) had very low SS and MS values. To get an f-value for an individual factor the Sum of Squares of a factor (SSF) is divided by the Sum of Squares of the error (SSE). Considering SSC has the largest value, it was expected to get a high value when dividing it by the small error term. Factor A and D are 2nd and 3rd in ranking order. Both Factors are much lower than Factor A, however they are still much higher than the critical f-value of 19 found from the critical f-value table (Figure 18. Appendix).

6. Conclusion

This thesis examines the creep response of Fused Filament Fabricated Polyethylene Terephthalate Glycol specimens by applying Taguchi's design of experiment method of optimization. The tensile specimens were designed according to standard ISO 527-2 [1A] printed using an Ender-3 S1 Pro and mechanically tested utilizing a X350-20 tensile machine.

The four printing parameters that were analysed: infill density (80%, 50% and 20%), infill orientation (90°, -45/45° and 0°), infill geometry (tri hexagonal, gyroid and cubic) with nozzle temperatures (220°C, 235°C and 250°C). The data from the tensile test was analysed by calculating the Signal-to-Noise ratio (smaller-is-better), creep modulus (MOC), instantaneous strain and Analysis of Variance (ANOVA).

The analysis concluded that the three samples with the highest creep modulus (8, 6 and 1) all had infill densities of 80 % with infill geometries of 1st cubic, 2nd gyroid and 3rd tri hexagonal. The weakest samples (3 and 5) have infill densities of 20% with the lowest modulus of creep. Sample 7, with 20% infill, had a higher modulus of creep than sample 4 with 50% infill. This is likely due to sample 4 having the weakest geometry (tri hexagonal) and sample 7 having the strongest geometry (cubic). A difference of 577.25 MPa strength between the strongest and the weakest samples.

The Signal-to-Noise ratio showed that an infill density of 80%, infill geometry cubic, infill orientation of -45/45° and with nozzle temperature 235 degrees Celsius are the optimal parameters for the best creep behavior. Furthermore, the parameters that yielded the worst SNR (poor creep behavior) were infill density of 20%, infill geometry gyroid, infill orientation of 0° and with nozzle temperature 250 degrees Celsius.

Finally, ANOVA provided insight into the % contribution that each factor had on the creep response. Factor A contributed 9.7% with an f-value of 97.97. Factor C contributed 85.6% with an f-value of 862.24. Factor D contributed 4.47% with an f-value of 45. Factor B was used as an error term due to lack of pure error and less than 0.1% overall contribution. Furthermore, factors A, C and D were all significant with $\alpha=0.05$, meaning each factor rejects the null hypothesis and are statistically significant.

This thesis has provided further insight into the creep behavior of 3D printed PETG, and the applications of utilizing the Taguchi method for design and optimization of 3D printed parts.

This research has given headway for further analysis of FFF PETG and the future applications for Tugushi's Design of Experiment. However, the accuracy of these results can be improved on. For example, adding more experimental repetition would create an error term that would substitute for factor B for improving overall accuracy of the ANOVA.

Future research should focus on larger factorial designs, and conformation studies. Simple and complex optimization research is essential for development and growth within businesses, manufacturing industries and institutes.

7. References

[1] Food and Agriculture Orginization United Nations, "Food and Agriculture Orginization United Nations," 2022. [Online]. Available: https://www.fao.org/3/cb9479en/online/sofa-2022/trends-drivers-motorized-mechanization.html.

[2] N. E. S. H. Masriadi Dasmadi, "Exploring the Future of Work: Impact of Automation and Artificial Intelligence on Employment," *ENDLESS International Journal of Future Studies,* vol. 6, no. 1, pp. 125-126, 2023.

[3] Artesans WP team in Omitsis, "www.bcn3d.com," BCN3D, 15 5 2020. [Online]. Available: https://www.bcn3d.com/the-history-of-3d-printing-when-was-3d-printing-invented/.

[4] L. K. L. K. Satabda Chaudhuri, "Impact of using ai in manufacturing industries," *Journal of the International Academy for Case Studies,* vol. 28, no. S4, pp. 1-10, 2022.

[5] C. Evans, "3D PRINTING MATERIALS," Fictiv, 17 8 2020. [Online]. Available: https://www.fictiv.com/materials/3d-printing-petg.

[6] C. K. A. T. V. S. G. S. D. S. V. D. Catherine Yan, "PETG: Applications in Modern Medicine," *Engineered Regeneration,* vol. 5, no. 1, pp. 45-55, 2024.

[7] K. T. D. &. A. A. M. Mansour, "Mechanical and Dynamic Behavior of Fused Filament Fabrication 3D Printed Polyethylene Terephthalate Glycol Reinforced with Carbon Fibers," *Polymer-Plastics Technology and Engineering ,* vol. 57, no. 16, pp. 1715-1725, 2018.

[8] A. P. S. P. R. Sara Valvez, "Compressive Behaviour of 3D-Printed PETG Composites," *Aerospace,* vol. 9, no. 3, p. 124, 2022.

[9] A. P, "A Closer Look at 3D Printing Materials: Plastics," 3D NAtive, 8 6 2023. [Online]. Available: https://www.3dnatives.com/en/plastics-used-3d-printing110420174/#!.

[10] Elegant Themes, "recycletheone.com," End the waste recylce 1, 28 2 2023. [Online]. Available: https://www.recycletheone.com/what-is-pet/.

[11] T. Boissonnealut, "Wevolver," 19 9 2023. [Online]. Available: https://www.wevolver.com/article/3d-printing-rafts-vs-brims-vs-skirts-how-to-get-started.

[12] F. A. d. A. G. F. G. Rhuan José Ribeiro Pereira, "A multiobjective optimization parameters applied to additive manufacturing: DOE-based approach to 3D printing," *ScienceDirect,* pp. 1710-1731, 2023.

[13] J. P. D. K. Arnošt Vespalec, "DoE Approach to Setting Input Parameters for Digital 3D Printing of Concrete for Coarse Aggregates up to 8 mm," *MDPI,* vol. 16, no. 9, pp. 3349-3356, 2023.

[14] R. G. R. D. a. T. Alexandra Ileana Portoacă, "Optimization of 3D Printing Parameters for Enhanced Surface Quality and Wear Resistance," *MDPI,* vol. 15, no. 16, pp. 3416-3425, 2023.

[15] L. E. P. L. H. R. Silas Z. Gebrehiwot, "Optimising the mechanical properties of additive-manufactured," *The International Journal of Advanced Manufacturing Technology,* p. 4909–4924, 29 june 2023.

[16] S. D. K. U. M. S. R. B. A. S. S. C. L. R. A. I. a. M. F. B. S. Ganeshkumar, "Investigation of Tensile Properties of Different Infill Pattern Structures of 3D-Printed PLA Polymers: Analysis and Validation Using Finite Element Analysis in ANSYS," *Materials (Basel),* vol. 15, no. 15, p. 5142, 2022.

[17] Matthew, "the-history-of-3d-printing-additive-manufacturing," Aditive-X, 2023.

[18] A. Chapman, "ultimaker.com," 3D Systems Corporation, 29 7 2022. [Online]. Available: https://ultimaker.com/learn/the-complete-history-of-3d-printing/.

[19] H. Zhang, "11-Building Plastic," *Building Materials in Civil Engineering,* vol. 423, pp. 289-303, 2011.

[20] C. W. B. K. J. B. Özgür Keleş, "Effect of build orientation on the mechanical reliability of 3D printed ABS," *Rapid Prototyping Journal,* 31 3 2016.

[21] RAHN AG, "rahen-group.com," RAHN, 11 8 2024. [Online]. Available: https://www.rahn-group.com/en/energycuring/3d-printing/what-is-vat-photopolymerization/.

[22] F. B. N. G. C. P. R. J. H. C. J. T. Nesma T. Aboulkhair, "CHAPTER 6- Additive manufacturing processes for metals," in *Additive manufacturing processes for metals*, 2023, pp. 201-258.

[23] R. Z. P. V. M. S. W. H. G. K. Z. Weiming Ji, "Recent progress in gradient-structured metals and alloys," *Progress in mterial science,* vol. 140, p. 101194, 12 2023.

[24] Formlabs, "Additive vs. Subtractive Manufacturing," Formlabs.com, 17 4 2024. [Online]. Available: https://formlabs.com/blog/additive-manufacturing-vs-subtractive-manufacturing/.

[25] Zintilon, "Subtractive vs Additive Manufacturing: Examining the Differences," Zintilon.com, 26 3 2023. [Online]. Available: https://www.zintilon.com/blog/subtractive-vs-additive-manufacturing/. [Accessed 11 8 2023].

[26] R. a. H. A. a. K. S. Shewbridge, "Everyday making: Identifying future uses for 3D printing in the home," *Proceedings of the Conference on Designing Interactive Systems: Processes, Practices, Methods, and Techniques, DIS,* 6 2014.

[27] University of Pittsburgh, "Why Commercialize?," 21 10 2020. [Online]. Available: https://www.innovation.pitt.edu/for-inventors/why-commercialize-at-pitt/. [Accessed 11 8 2024].

[28] J. Bergström, 11 - Material Modeling Case Studies, William Andrew, 2015, pp. 455-497.

[29] A. Wells, "https://plastiquarian.com/," 5 7 2024. [Online]. Available: https://plastiquarian.com/?page_id=14270. [Accessed 13 8 2024].

[30] Univeristy of Colorado Boulder, "College of arts and science," 23 12 2015. [Online]. Available: https://www.colorado.edu/lab/lecture-demo-manual/o670-polymerization-synthesis-nylon. [Accessed 13 8 2024].

[31] B. S. T. Lee Tin Sin, "1 - Plastics and environmental sustainability issues," *Plastics and Sustainability practical approaches,* vol. 60, no. 1, pp. 1-43, 2023.

[32] TWI-global, "TWI-global.com," 7 12 2020. [Online]. Available: https://www.twi-global.com/technical-knowledge/faqs/what-is-petg. [Accessed 13 8 2024].

[33] Any Shape Plastics, "what-is-polyethylene-terephthalate-glycol-petg," 31 1 2024. [Online]. Available: https://anyshapeplastics.com.au/what-is-polyethylene-terephthalate-glycol-petg/. [Accessed 13 8 2024].

[34] H.-Y. K. F.-L. J. S.-J. P. Ho-Ju Bang, "Fibers spun from 1,4-cyclohexanedimethanol-modified polyethylene terephthalate resin," *Journal of Industrial and Engineering Chemistry,* vol. 17, no. 4, pp. 805-810, 2011.

[35] UN Environment, "UNEP - UN Environment Programme," 2 8 2022. [Online]. Available: https://www.unep.org/plastic-pollution. [Accessed 13 8 2024].

[36] NOAA, "National Oceanic and Atmospheric Administration," United states government , 13 4 2016. [Online]. Available: https://oceanservice.noaa.gov/facts/microplastics.html. [Accessed 13 8 2024].

[37] E. Çakmakçi, "Chapter 8 - POSS—Thermosetting polymer nanocomposites," in *Polyhedral Oligomeric Silsesquioxane (POSS) Polymer Nanocomposites*, Kottayam, Elsevier, 2021, pp. 127-175.

[38] Advanced Plastiform, "advancedplastiform.com," 17 12 2019. [Online]. Available: https://advancedplastiform.com/thermoplastics-vs-thermoset-materials/. [Accessed 13 8 2024].

[39] S. F. K. E. H. F. Mohammadjavad Kazemi, "State of the art in recycling waste thermoplastics and thermosets and their applications in construction," *Resources, Conservation and Recycling,* vol. 174, p. 105776, 11 2021.

[40] M. Jones, "all3dp.com," 25 7 2018. [Online]. Available: https://all3dp.com/2/3d-printer-recycled-plastic-tips-for-your-waste-plastic/. [Accessed 13 8 2024].

[41] Team Xometry, "Xometry where big ideas are built," 19 9 2020. [Online]. Available: https://www.xometry.com/resources/3d-printing/petg-3d-printing-filament/. [Accessed 13 8 2024].

[42] T. Polygenis, "PETG vs PLA: Differences and Comparison," *Wevolver,* 1 12 2023.

[43] Phillip Chesser, "protomaker3d," 20 3 2023. [Online]. Available: https://protomaker3d.com/blogs/learn/clear-petg-in-3d-printing-properties-and-applications. [Accessed 13 8 2024].

[44] twi-global, "twi-global.com," 7 12 2020. [Online]. Available: https://www.twi-global.com/technical-knowledge/faqs/what-is-petg. [Accessed 4 12 2024].

[45] Kara, "additive-x.com," 3 12 2021. [Online]. Available: https://additive-x.com/blog/what-is-infill-what-does-it-do/. [Accessed 13 8 2024].

[46] R. A. Shivani Sriya Ambati, "Effect of infill density and infill pattern on the mechanical properties of," *Materials Today: Proceedings,* vol. 64, no. 1, pp. 804-807, 2022.

[47] L. &. V. M. &. S. L. &. A. L. Bergonzi, "Different infill geometry influence on mechanical properties of FDM produced PLA Different infill geometry influence on mechanical properties of FDM produced PLA," *IOP Conference Series Materials Science and Engineering,* vol. 1038, 2021.

[48] H. G. T. T. M. C. J. L. N. A. F. S. J. Z. T. H. B. B. N.-C. James M. Ennis, "ffects of infill orientation and percentage on the magnetoactive properties of 3D printed magnetic elastomer structures," *dditive Manufacturing Letters,* vol. 4, no. 100109, pp. 2772-3690, 2023.

[49] D. T. S. C. Mahesh Naik, "An insight into the effect of printing orientation on tensile strength of multi-infill pattern 3D printed specimen: Experimental study," *Materialstoday:PROCEEDINGS,* vol. 62, no. 14, pp. 7391-7395, 2022.

[50] F. V.-T. M.-A. S.-S. Mohammad Reza Adibeig, "Numerical and experimental investigation on creep response of 3D printed Polylactic acid (PLA) samples. Part I: The effect of building direction and unidirectional raster orientation," *Journal of the Mechanical Behavior of Biomedical Materials,* vol. 145, 2023.

[51] G. L. D. X. F. L. Shenglong Jiang, "Mechanical properties analysis of polyetherimide parts fabricated by fused deposition modeling," *High Performance Polymers,* vol. 31, no. 1, p. 095400831775282, 2018.

[52] J. O'Connell, "All3DP.pro," ALL3DP.com, 31 12 2023. [Online]. Available: https://all3dp.com/2/infill-3d-printing-what-it-means-and-how-to-use-it/. [Accessed 4 12 2024].

[53] J. O'Connell, "all3dp.com," 31 12 2023. [Online]. Available: https://all3dp.com/2/infill-3d-printing-what-it-means-and-how-to-use-it/. [Accessed 14 8 2024].

[54] M. Biron, "8 - Thermal Properties," in *Material Selection for Thermoplastic Parts*, William Andrew, 2016, pp. 339-375.

[55] A. a. Y. Morteza Behzadnasa, "Effects of 3D printer nozzle head temperature on the physical and mechanical properties of PLA based product," in *12th International Seminar on Polymer Science and Technology*, Tehran, 2016.

[56] L. McKeen, "3 - Introduction to the Physical, Mechanical, and Thermal Properties of Plastics and Elastomers," *The Effect of Sterilization on Plastics and Elastomers,* vol. third edition, pp. 57-84, 2012.

[57] Z. Hay, "All3dp.com," 5 12 2023. [Online]. Available: https://all3dp.com/2/the-best-printing-temperature-for-different-filaments/. [Accessed 14 8 2024].

[58] L. Z. a. Y. W. a. M. N. a. E. P. a. Y. Y. a. J. P. a. D. C. a. J. Qiao, "Creep deformation in metallic glasses: A global approach with strain as an indicator within transition state theory," *International Journal of Plasticity,* vol. 174, no. 0749-6419, p. 103923, 2024.

[59] corrosionpedia, "corrosionpedia.com," 19 7 2024. [Online]. Available: https://www.corrosionpedia.com/definition/6175/creep-failure. [Accessed 14 8 2024].

[60] SIMSCALE, "simscale.com," 7 3 2024. [Online]. Available: https://www.simscale.com/docs/simulation-setup/materials/creep/. [Accessed 14 8 2024].

[61] S. V. Mostafa Katouzian, "Creep Response of Neat and Carbon-Fiber-Reinforced PEEK and Epoxy Determined Using a Micromechanical Model," *Composite Structures with Symmetry,* vol. 12, no. 10, p. 1680, 2020.

[62] M. Billen, "geo.libretexts.org," 9 7 2020. [Online]. Available: https://geo.libretexts.org/Courses/University_of_California_Davis/GEL_056%3A_Introduction_to_Geophysics/Geophysics_is_everywhere_in_geology.../01%3A_Rheology_of_Rocks/1.02%3A_Strain_and_Strain_Rate. [Accessed 14 8 2024].

[63] M. Biron, "7 - Advanced Environmental and Engineering Properties to Support Eco-Design for Plastics," *In Plastics Design Library,* pp. 309-369, 2020.

[64] ASQ, "ASQ - Excellence Through Quality," [Online]. Available: https://asq.org/about-asq/honorary-members/taguchi. [Accessed 19 8 2024].

[65] W. Kenton, "Investopedia," 7 28 2024. [Online]. Available: https://www.investopedia.com/terms/t/taguchi-method-of-quality-control.asp. [Accessed 4 12 2024].

[66] W. &. A. N. &. K. F. A. &. H. A. &. H. S. K. &. N. A. &. K. W. &. A. M. Lestari, "Optimization of 3D printed parameters for socket prosthetic manufacturing using the taguchi method and response surface methodology," *Results in Engineering,* vol. 21, p. 101847, 2024.

[67] M. &. N. F. Wicaksono, "Optimization of 3D Printing Parameters Using the Taguchi Method to Improve Dimensional Precision," *Jurnal Teknologi,* pp. 13-18, 2022.

[68] J. Z. M. O. B. T. Stephanie Fraley, "Design of Experiments via Taguchi Methods - Orthogonal Arrays," *LibreTexts.org,* 19 05 2020.

[69] Cadence PCB Solutions, "resources.pcb.cadence.com," 17 7 2024. [Online]. Available: https://resources.pcb.cadence.com/blog/2020-what-is-signal-to-noise-ratio-and-how-to-calculate-it. [Accessed 19 8 2024].

[70] T. K. Kim, "Understanding one-way ANOVA using conceptual figures," *Korean J Anesthesiol,* vol. 70, no. 1, pp. 22-26, 2017.

[71] W. Kenton, "Investopdeia," 30 7 2024. [Online]. Available: https://www.investopedia.com/terms/a/anova.asp. [Accessed 19 8 2024].

[72] M. A. T. Q. A. G. Adel Mahmood Hassan, "Statistical analysis of some mechanical properties of friction stir welded aluminium matrix composite," *International Journal of Experimental Design and Process Optimisation,* vol. 3, pp. 91-109, 2012.

[73] S. R. M. A. F. B. Atefeh Rajabi Kafshgar, "Optimization of Properties for 3D Printed PLA Material Using Taguchi, ANOVA and Multi-Objective Methodologies," *Procedia Structural Integrity,* vol. 34, pp. 71-77, 2021.

[74] AUTODESK, "Autodesk.com," 25 2 2021. [Online]. Available: https://www.autodesk.com/solutions/cad-software. [Accessed 21 8 2024].

[75] SOLIDWORKS Corp, "solidworks.com," 28 3 2024. [Online]. Available: https://www.solidworks.com/product/solidworks-3d-cad?gad_source=1&gclid=CjwKCAjwoJa2BhBPEiwA0l0ImKDopD4pIQVYEH8i9-1iq-lM3j05x57VIE2kA8LCFJ6iSAH6KTm-SBoCePsQAvD_BwE. [Accessed 21 8 2024].

[76] SIMPLIFY3D, "Simplify3d.com," 31 5 2019. [Online]. Available: https://www.simplify3d.com/resources/articles/rafts-skirts-and-brims/. [Accessed 25 8 2024].

[77] D. Navarro, "Factorial ANOVA 1- Balanced Designs, No Interactions," LibreTexts, 8 1 2024. [Online]. Available: https://stats.libretexts.org/Bookshelves/Applied_Statistics/Learning_Statistics_with_R_-_A_tutorial_for_Psychology_Students_and_other_Beginners_(Navarro)/16%3A_Factorial_ANOVA/16.01%3A__Factorial_ANOVA_1-_Balanced_Designs_No_Interactions. [Accessed 16 7 2024].

[78] Devils Design Products, "Devils Design Products," Devils Design, 20 5 2024. [Online]. Available: https://devildesign.com/. [Accessed 16 7 2024].

[79] "Ulti Maker," 29 4 2023. [Online]. Available: https://ultimaker.com/3d-printers/s-series/ultimaker-s3/. [Accessed 16 7 2024].

[80] P. Ghosh, "ResearchGate," 5 6 2016. [Online]. Available: https://www.researchgate.net/post/How-to-calculate-percentage-contribution-values-of-different-factors-in-Plackett-Burman-Design-including-Center-Points. [Accessed 11 11 2024].

[81] Y. L. Y. Z. Y. L. Yeyuan Hu, "Influence of Cooling Rate on Crystallization Behavior of Semi-Crystalline Polypropylene: Experiments and Mathematical Modeling," *Polymers,* vol. 14, p. 3646, 9 2022.

[82] Z. Bobbit, "STATOLOGY," 27 5 2019. [Online]. Available: https://www.statology.org/how-to-read-the-f-distribution-table/. [Accessed 13 11 2024].

[83] "How AI is transforming factories," *SANDVIK,* 28 4 2023.

[84] StudySmarter, "StudySmarter.co.uk," Materials engineering, 4 4 2023. [Online]. Available: https://www.studysmarter.co.uk/explanations/engineering/materials-engineering/stages-of-creep/.

[85] GAP Polymers, "www.gap-polymers.com," GAP Polymers, 2023. [Online]. Available: https://www.gap-polymers.com/en/blog-post/pet-vs-petg.

[86] M. M. H. V. V. A. H. Z. S. I. O. Rawabe Fatima Faidallah, "Effect of Different Standard Geometry Shapes on the Tensile Properties of 3D-Printed Polymer," *Polymers,* vol. 15, no. 14, p. 3029, 2023.

[87] R. &. A. I. &. A. D. T. &. B. D. Ferreira, "Experimental characterization and micrography of 3D printed PLA and PLA reinforced with short carbon fibers," *Composites Part B: Engineering,* vol. 124, 2017.

Appendices

[82]

	DF1	α = 0.05																	
DF2	1	2	3	4	5	6	7	8	9	10	12	15	20	24	30	40	60	120	Inf
1	161.45	199.5	215.71	224.58	230.16	233.99	236.77	238.88	240.54	241.88	243.91	245.95	248.01	249.05	250.1	251.14	252.2	253.25	254.31
2	18.513	19	19.164	19.247	19.296	19.33	19.353	19.371	19.385	19.396	19.413	19.429	19.446	19.454	19.462	19.471	19.479	19.487	19.496
3	10.128	9.5521	9.2766	9.1172	9.0135	8.9406	8.8867	8.8452	8.8123	8.7855	8.7446	8.7029	8.6602	8.6385	8.6166	8.5944	8.572	8.5494	8.5264
4	7.7086	6.9443	6.5914	6.3882	6.2561	6.1631	6.0942	6.041	5.9988	5.9644	5.9117	5.8578	5.8025	5.7744	5.7459	5.717	5.6877	5.6581	5.6281
5	6.6079	5.7861	5.4095	5.1922	5.0503	4.9503	4.8759	4.8183	4.7725	4.7351	4.6777	4.6188	4.5581	4.5272	4.4957	4.4638	4.4314	4.3985	4.365
6	5.9874	5.1433	4.7571	4.5337	4.3874	4.2839	4.2067	4.1468	4.099	4.06	3.9999	3.9381	3.8742	3.8415	3.8082	3.7743	3.7398	3.7047	3.6689
7	5.5914	4.7374	4.3468	4.1203	3.9715	3.866	3.787	3.7257	3.6767	3.6365	3.5747	3.5107	3.4445	3.4105	3.3758	3.3404	3.3043	3.2674	3.2298
8	5.3177	4.459	4.0662	3.8379	3.6875	3.5806	3.5005	3.4381	3.3881	3.3472	3.2839	3.2184	3.1503	3.1152	3.0794	3.0428	3.0053	2.9669	2.9276
9	5.1174	4.2565	3.8625	3.6331	3.4817	3.3738	3.2927	3.2296	3.1789	3.1373	3.0729	3.0061	2.9365	2.9005	2.8637	2.8259	2.7872	2.7475	2.7067
10	4.9646	4.1028	3.7083	3.478	3.3258	3.2172	3.1355	3.0717	3.0204	2.9782	2.913	2.845	2.774	2.7372	2.6996	2.6609	2.6211	2.5801	2.5379
11	4.8443	3.9823	3.5874	3.3567	3.2039	3.0946	3.0123	2.948	2.8962	2.8536	2.7876	2.7186	2.6464	2.609	2.5705	2.5309	2.4901	2.448	2.4045
12	4.7472	3.8853	3.4903	3.2592	3.1059	2.9961	2.9134	2.8486	2.7964	2.7534	2.6866	2.6169	2.5436	2.5055	2.4663	2.4259	2.3842	2.341	2.2962
13	4.6672	3.8056	3.4105	3.1791	3.0254	2.9153	2.8321	2.7669	2.7144	2.671	2.6037	2.5331	2.4589	2.4202	2.3803	2.3392	2.2966	2.2524	2.2064
14	4.6001	3.7389	3.3439	3.1122	2.9582	2.8477	2.7642	2.6987	2.6458	2.6022	2.5342	2.463	2.3879	2.3487	2.3082	2.2664	2.2229	2.1778	2.1307
15	4.5431	3.6823	3.2874	3.0556	2.9013	2.7905	2.7066	2.6408	2.5876	2.5437	2.4753	2.4034	2.3275	2.2878	2.2468	2.2043	2.1601	2.1141	2.0658
16	4.494	3.6337	3.2389	3.0069	2.8524	2.7413	2.6572	2.5911	2.5377	2.4935	2.4247	2.3522	2.2756	2.2354	2.1938	2.1507	2.1058	2.0589	2.0096
17	4.4513	3.5915	3.1968	2.9647	2.81	2.6987	2.6143	2.548	2.4943	2.4499	2.3807	2.3077	2.2304	2.1898	2.1477	2.104	2.0584	2.0107	1.9604
18	4.4139	3.5546	3.1599	2.9277	2.7729	2.6613	2.5767	2.5102	2.4563	2.4117	2.3421	2.2686	2.1906	2.1497	2.1071	2.0629	2.0166	1.9681	1.9168
19	4.3807	3.5219	3.1274	2.8951	2.7401	2.6283	2.5435	2.4768	2.4227	2.3779	2.308	2.2341	2.1555	2.1141	2.0712	2.0264	1.9795	1.9302	1.878
20	4.3512	3.4928	3.0984	2.8661	2.7109	2.599	2.514	2.4471	2.3928	2.3479	2.2776	2.2033	2.1242	2.0825	2.0391	1.9938	1.9464	1.8963	1.8432
21	4.3248	3.4668	3.0725	2.8401	2.6848	2.5727	2.4876	2.4205	2.366	2.321	2.2504	2.1757	2.096	2.054	2.0102	1.9645	1.9165	1.8657	1.8117
22	4.3009	3.4434	3.0491	2.8167	2.6613	2.5491	2.4638	2.3965	2.3419	2.2967	2.2258	2.1508	2.0707	2.0283	1.9842	1.938	1.8894	1.838	1.7831
23	4.2793	3.4221	3.028	2.7955	2.64	2.5277	2.4422	2.3748	2.3201	2.2747	2.2036	2.1282	2.0476	2.005	1.9605	1.9139	1.8648	1.8128	1.757
24	4.2597	3.4028	3.0088	2.7763	2.6207	2.5082	2.4226	2.3551	2.3002	2.2547	2.1834	2.1077	2.0267	1.9838	1.939	1.892	1.8424	1.7896	1.733
25	4.2417	3.3852	2.9912	2.7587	2.603	2.4904	2.4047	2.3371	2.2821	2.2365	2.1649	2.0889	2.0075	1.9643	1.9192	1.8718	1.8217	1.7684	1.711
26	4.2252	3.369	2.9752	2.7426	2.5868	2.4741	2.3883	2.3205	2.2655	2.2197	2.1479	2.0716	1.9898	1.9464	1.901	1.8533	1.8027	1.7488	1.6906
27	4.21	3.3541	2.9604	2.7278	2.5719	2.4591	2.3732	2.3053	2.2501	2.2043	2.1323	2.0558	1.9736	1.9299	1.8842	1.8361	1.7851	1.7306	1.6717
28	4.196	3.3404	2.9467	2.7141	2.5581	2.4453	2.3593	2.2913	2.236	2.19	2.1179	2.0411	1.9586	1.9147	1.8687	1.8203	1.7689	1.7138	1.6541
29	4.183	3.3277	2.934	2.7014	2.5454	2.4324	2.3463	2.2783	2.2229	2.1768	2.1045	2.0275	1.9446	1.9005	1.8543	1.8055	1.7537	1.6981	1.6376
30	4.1709	3.3158	2.9223	2.6896	2.5336	2.4205	2.3343	2.2662	2.2107	2.1646	2.0921	2.0148	1.9317	1.8874	1.8409	1.7918	1.7396	1.6835	1.6223
40	4.0847	3.2317	2.8387	2.606	2.4495	2.3359	2.249	2.1802	2.124	2.0772	2.0035	1.9245	1.8389	1.7929	1.7444	1.6928	1.6373	1.5766	1.5089
60	4.0012	3.1504	2.7581	2.5252	2.3683	2.2541	2.1665	2.097	2.0401	1.9926	1.9174	1.8364	1.748	1.7001	1.6491	1.5943	1.5343	1.4673	1.3893
120	3.9201	3.0718	2.6802	2.4472	2.2899	2.175	2.0868	2.0164	1.9588	1.9105	1.8337	1.7505	1.6587	1.6084	1.5543	1.4952	1.429	1.3519	1.2539
Inf	3.8415	2.9957	2.6049	2.3719	2.2141	2.0986	2.0096	1.9384	1.8799	1.8307	1.7522	1.6664	1.5705	1.5173	1.4591	1.394	1.318	1.2214	1

Figure 18 Critical F-value table p.52